ISTANBUL TECHNICAL UNIVERSITY ★ GRADUATE SCHOOL OF SCIENCE ENGINEERING AND TECHNOLOGY

INVESTIGATION OF THE MISFOLDING PATHWAY OF DIFFERENT PRION VARIANTS VIA MOLECULAR DYNAMICS SIMULATIONS

M.Sc. THESIS

Fulya Ecem KESKİN

Department of Moleculear Biology, Genetics and Biotechnology

Molecular Biology, Genetics and Biotechnology Programme

SEPTEMBER, 2015

ISTANBUL TECHNICAL UNIVERSITY ★ GRADUATE SCHOOL OF SCIENCE ENGINEERING AND TECHNOLOGY

INVESTIGATION OF THE MISFOLDING PATHWAY OF DIFFERENT PRION VARIANTS VIA MOLECULAR DYNAMICS SIMULATIONS

M.Sc. THESIS

Fulya Ecem KESKİN
521121136

Department of Molecular Biology, Genetics and Biotechnology

Molecular Biology, Genetics and Biotechnology Programme

Thesis Advisor: Asistant Prof. Dr. Bülent BALTA

SEPTEMBER, 2015

İSTANBUL TEKNİK ÜNİVERSİTESİ ★ FEN BİLİMLERİ ENSTİTÜSÜ

FARKLI PRION PROTEİNİ VARYANTLARININ YANLIŞ KATLANMA MEKANİZMALARININ MOLEKÜLER DİNAMİK SİMÜLASYONLARI İLE ARAŞTIRILMASI

YÜKSEK LİSANS TEZİ

Fulya Ecem KESKİN
(521121136)

Moleküler Biyoloji, Genetik ve Biyoteknoloji Anabilim Dalı

Moleküler Biyoloji, Genetik ve Biyoteknoloji Programı

Tez Danışmanı: Yardımcı Doç. Dr. Bülent BALTA

EYLÜL, 2015

Fulya Ecem KESKİN, a M.Sc**.** student of ITU Graduate School of Molecular Biology, Genetics and Biotechnology student ID 521121136, successfully defended the thesis entitled "INVESTIGATION OF THE MISFOLDING PATHWAY OF DIFFERENT PRION VARIANTS VIA MOLECULAR DYNAMICS SIMULATIONS", which she prepared after fulfilling the requirements specified in the associated legislations, before the jury whose signatures are below.

Thesis Advisor :	**Asistant Prof. Bülent BALTA** İstanbul Technical University	.....
Jury Members :	**Asistant Prof. Bülent BALTA** İstanbul Technical University	.....
	Associate Prof. Alimet Sema ÖZEN Piri Reis University	.....
	Associate Prof. F. Aylin KONUKLAR Istanbul Technical University	.....

Date of Submission : 04 September 2015
Date of Defense : 30.09.2015

To my all preciouses,

FOREWORD

As a veterinary doctor I have had macro vision on diseases. My main goal on this master study is to gain a micro vision and develop a different approach by merging my macro vision with this micro vision.

During my master study, I have gained strong micro vision and this new vision helped me to develop a versatile approach. Thus, the way that I think and analyse diseases changed completely.

Prion subject is highly related with both veterinary discipline and molecular biology discipline. Therefore, studying on prions is a perfect match for my background.

In this study, I have had chance to implement my new vision which is the key to achieve important results.

I would like to express my sincere gratitude to my thesis advisor Asst. Prof. Dr. Bülent BALTA for his excellent support and guidance during my study. I have learnt a lot from him. He gave me the most important inputs to create my vision and develop this study.

I would also thank you to my family and all close friends for their continuous support and strong love.

May 2015

Fulya Ecem KESKİN
Veterinerian Doctor

TABLE OF CONTENTS

Page

FOREWORD ..... **ix**
TABLE OF CONTENTS ..... **xi**
ABBREVIATIONS ..... **xiii**
LIST OF FIGURES ..... **xv**
SUMMARY ..... **xvii**
ÖZET ..... **xx**
1. INTRODUCTION **1**
1.1 Transmissible Spongiform Encephalopathies in Humans and Other Animals .. 1
1.2 Search for the Cause of TSEs 2
1.3 Prions 3
1.4 MD Simulations in Literature 5
1.5 Aim of This Study 7
2. METHODOLOGY **9**
2.1 Force Fields 9
2.1.1 Stretching and bending 11
2.1.2 Torsion 11
2.1.3 Non-bonded interactions 12
2.2 Theory of Molecular Dynamics 13
2.3 Simulation Parameters 14
3. RESULTS AND DISCUSSIONS **17**
3.1 Simulations at 310K 17
3.1.1 Stability of simulations at 310 K as displayed by the root mean square deviations (RMSD) 17
3.1.2 Mobility of the residues 19
3.1.3 Cluster analysis 22
3.2 Detailed Analysis of the Simulations at 310K 27
3.2.1 The effect of Q/R variation at position 171 27
3.2.2 Structure of H1 and H1-B1 loop 28
3.2.3 Structure of the β-sheet in the neighbourhood of A/V136 33
3.2.4 The banana peeling model and current simulations 39
3.3 Additional Simulations at 310K 40
3.3.1 Restrained simulations forcing β-sheet formation 40
3.3.2 A136V mutation in ARR and V136A mutation in VRQ 41
3.4 Simulations at 330K 42
4. CONCLUSION AND RECOMMENDATIONS **43**
REFERENCES **45**
CURRICULUM VITAE **49**

ABBREVIATIONS

$\mathbf{A_{ij}}$	: van der Waals parameter
B	: Number of times the property is sampled
$\mathbf{B_{ij}}$	: van der Waals parameter
E	: Potential energy
$\mathbf{E_b}$	: Energy for bond angle
$\mathbf{E_{nb}}$	: Energy for non-bonded interactions
$\mathbf{E_s}$	: Energy for bond stretching
$\mathbf{E_\omega}$	: Torsional energy
F	: Force
F(k)	: Force vector
f(r)	: Conservative force acting on the particle
$\mathbf{k_b}$	: Force constant for bending
$\mathbf{k_s}$	: Force constant for strectching
l	: Actual bond length
$\mathbf{l_0}$	: Assigned bond length
M	: Total number of bond angles
m	: Mass
N	: Total number of bonds
p	: Momentum
$\mathbf{PrP^c}$	: Correctly folded prion protein
$\mathbf{PrP^{sc}}$	: Misfolded prion protein
q	: Phase point
$\mathbf{q_i}$	: Partial charge on atom i
$\mathbf{q_j}$	: Partial charge on atom j
$\mathbf{r_{ij}}$	: Distance between atom i and j
T	: Absolute temperature
v	: Velocity
x	: Position vector in 3N dimensional space
γ	: Phase factor
ε	: Dielectric constant of medium
BSE	: Bovine Spongiform Encephalopathy
CJD	: Creutzfeldt–Jakob Disease
FFI	: Fatal familiar insomnia
HIE	: Imidazole ring of His bears an hydrogen atom on Nε.
HIP	: Imidazole ring of His bears two hydrogen atoms on both Nδ and Nε.
HIS	: Histidine
Lys	: Lysine
MD	: Molecular dynamics
PDB	: Protein Data Bank
PMEMD	: Particle mesh ewald molecular dynamics
Q	: Glutamine
R	: Arginine

RF : Release Factor
Thr : Threonine
TME : Transmissible Mink Encephalopathy
TSE : Transmissible Spongiform Encephalopathy
UFF : Universal Force Field
V : Valine

LIST OF FIGURES

Page

Figure 1.1 : Crystallographic structure of the C-terminal part of PrPC 4
Figure 1.2 : Spontaneous transition to prion fold mechanism. 5
Figure 1.3 : Cerebellum of a sheep with atypical scrapie, vacuolizations of neurons. 5
Figure 1.4 : β-rich folds . Panel 0 shows NMR structure, Panel 11 shows the maximal β-content structure obtained in simulation [27]. 6
Figure 2.1 : Force field contributors. 10
Figure 3.1 : RMSD with respect to time for ARR at 310 K. 17
Figure 3.2 : RMSD with respect to time for ARQ at 310 K. 18
Figure 3.3 : RMSD with respect to time for VRQ at 310 K. 18
Figure 3.4 : B-factors ($Å^2$) in the ARR simulation at 310 K 20
Figure 3.5 : B-factors (A^2) in the ARQ simulation at 310 K. 20
Figure 3.6 : B-factors ($Å^2$) in the VRQ simulation at 310 K. 21
Figure 3.7 : Residues with high mobility. Pink: residues 135-149; blue: residues 168-177; yellow: residues 186-204. 21
Figure 3.8 : C terminal part of H2 and the loop connecting H2 to H3 where rich in threonine shows high flexibility. 22
Figure 3.9 : Clusters of ARR using a 4 Å radius (green: cluster 0, blue: cluster1, pink: cluster2). 23
Figure 3.10 : Clusters and cluster members of ARR with respect to time. 23
Figure 3.11 : Clusters of ARQ using 4 Å radius (green: cluster 0, blue: cluster1, pink: cluster2). 24
Figure 3.12 : Clusters and cluster members of ARQ with respect to time. 24
Figure 3.13 : Clusters of VRQ using 4 Å radius. 25
Figure 3.14 : Green: similar to crystal position (cluster 3); Pink: H1 rotates away from H3 (cluster 10) ; Purple: H1 move towards the C terminus (cluster 6). 25
Figure 3.15 : Time evolution of the position of H1 in VRQ simulation. (Yellow: cluster 3; Green: cluster 0; Cyan: cluster 1; Purple: cluster 6; Pink: cluster 2; Salmon: cluster4.) 26
Figure 3.16 : Clusters and Cluster Members of VRQ with respect to time. 27
Figure 3.17 : Respectively ARR, ARQ, VRQ simulations and the positions of the residues D170 and R/Q171. 28
Figure 3.18 : Interactions between H1, H3 and H1-B1 H3 Loop in the crystallographic structure. 29
Figure 3.19 : Interactions in ARQ after K207-E149 and I142-V212 are replaced by E149-R211 and P140-V212. 29
Figure 3.20 : R154-D150 and R151-D147 salt bridges maintain the stability of the N-terminal turns of H1. 30
Figure 3.21 : Salt bridge between R139-D150 and formation of 3_{10} helix. 31

Figure 3.22 : Interactions between H1and H3 or H1-B1 loop and H3 when the 3_{10} helix is formed. 32
Figure 3.23 : Interactions in the very open conformation. 32
Figure 3.24 : Interaction preventing (A) or favoring (B) the formation of 3_{10} helix. 33
Figure 3.25 : Hydrogen bond between A136-N162. Alanin can fit into the space between M216 and Q220. 34
Figure 3.26 : Alanine in a partially solvent exposed conformation. 34
Figure 3.27 : Hydrogen bond is seen between N162 and NH group of M137 in fully solvent exposed conformation of alanine. 35
Figure 3.28 : V136 located in the solution. 36
Figure 3.29 : Beta turn formation in very open conformation. 36
Figure 3.30 : Hydrogen bond is between Q220 and V136 in very open conformation of valine. 37
Figure 3.31 : Hydrogen bond is between M137 and Q220. 37
Figure 3.32 : Hydrogen bond is between S138 and N162. 38
Figure 3.33 : Hydrophobic interactions are between Y160 and P140. 38
Figure 3.34 : Valine in the burried conformation in very open conformation. 39
Figure 3.35 : H2, H3 and H2-H3 loop during simulation. 40
Figure 3.36 : Restrained regions in VRQ : 1) G198 NH – T194 CO (yellow-pink) 2) G198 CO – T194 NH 3) N200 NH – V192 CO (blue-purple) 41
Figure 3.37 : Restrain regions in VRQ: 1) R159 CO – T194 NH (blue-salmon) 2) R159 NH – T194 CO 41

INVESTIGATION OF THE MISFOLDING PATHWAY OF DIFFERENT PRION VARIANTS VIA MOLECULAR DYNAMICS SIMULATIONS

SUMMARY

Transmissible Spongiform Encephalopathies(TSE) are fatal neurodegenerative diseases. Examples are: bovine spongiform encephalopathy (BSE) in cow, scrapie in sheep and Creutzfeldt Jakob disease (CJD) in humans. A misfolded version of a protein named prion causes these diseases.

Properly folded protein(PrP^{C}) is rich of α-helix. The misfolded protein (PrP^{Sc}) contains less α-helix and is mostly comprised of β-sheets. Encounter of PrP^{C} and PrP^{Sc} catalyzes the misfolding and disease propagation. The disease is transferred between individuals via transfer of these proteins. PrP^{Sc} can create oligomers or fibrils.

The N-terminus of this protein is disordered and it is believed that it binds Cu^{2+}. The ordered part at the C-terminus is comprised of 3 α-helices and 2 β-strands in the correctly folded state. In the literature, the part of the protein which causes the disease is controversial. Also, the misfolded shape and misfoling pathways are unknown. The predominantly accepted idea is that helices 2 and 3 (H2 and H3) at the C-terminus create a β-sheet by misfolding. Existance of more than one misfolded shape and pathway is also possible. However, the 3-dimensional PrP^{Sc} shape is still unknown and there is a need for researches on this subject.

This study will contribute to enlighting of these misfolding pathways by using molecular dynamic simulations.

One of the most common form of TSE is scrapie. For scrapie development, the 136th, 154th and 171st residues are important. This study focuses on 3 variants. First of these variants is weakly resistant wild type (ARQ: A136, R154, Q171), the second one is the most susceptible mutant (VRQ: V136, R154, Q171) and the other one is the most resistant mutant (ARR: A136, R154, R171).

Simulations have been made with generalized Born continuum solvation method and Amber ff10 force field at 310 and 330 Kelvin. Simulation durations are 400-700ns. Fluctuated regions (except termini) of the proteins in all 3 simulations at 310K are: 1) H1 and the loop between H1 and β-strand 1(residues 135-149); 2) the loop between β-strand 2 and H2 (residues 168-177); 3) C-terminus of H2 and the loop between H2 and H3 (residues 186-204). Movement of the region between 168-177 is similiar in all 3 variants. In the other two regions, the magnitude and direction of the movements are found to be different in all 3 variants. ARR which is the most resistant variant has the lowest mobility. VRQ, the most susceptible variant, is the most mobile variant in the simulations. Therefore, it is seen that there is a relation between susceptibility and mobility. Especially, in VRQ, H1 is relocated with respect to H3.

Position of H1 in the other two variants (ARR, ARQ) is not too far from crystal structures. Hence it is seen that valine as the 136th residue has an effect regarding the reposition of H1. The other two variants have alanine instead of valine as the 136th residue.

In order to accelerate the conformational changes, simulations have been performed at 330 K and H1 has changed its position in all these simulations, including ARR and ARQ. In addition, VRQ has deformed its β-sheet in the 330 K simulations. These results are compatible with the 'banana peeling model' which suggests that relocation of H1 is necessary for the conversion of H2 and H3 to β-sheet.

FARKLI PRION PROTEİNİ VARYANTLARININ YANLIŞ KATLANMA MEKANİZMALARININ MOLEKÜLER DİNAMİK SİMÜLASYONLARI İLE ARAŞTIRILMASI

ÖZET

Bulaşıcı süngerimsi ensefalopatiler (TSE) ölümcül nörodejeneratif hastalıklardır. İnsanda; Creutzfeldt Jakob hastalığı (CJD), Fatal Familial İnsomnia (FFI), hayvanlarda; Bovine Spongiform Encephalopathy (BSE), skrapi, Transmissible Mink Encephalopathy (TME) gibi hastalıklara prion adı verilen bir proteinin yanlış katlanması neden olur.

Creutzfeldt Jakob Disease (CJD): Tedavi edilmeyen ölümcül bir hastalıktır. Kendini bunama, hafıza kaybı, halüsinasyonlar ve anksiyete ile gösterir. Deli dana olarak bilinen Bovine Spongiform Encephalopathy'nin insanlardaki formudur.

Fatal Familial Insomnia (FFI): Dünyada 40 ailede bulunan bir hastalıktır. Hastalar uyuyamama, hızlı kilo kaybının yanı sıra halüsinasyon ve bunama gösterir, hastayı ölüme doğru götürür.

Gerstmann- Straussler-Scheinker sendromu çok az görülen bir hastalıktır. Konuşma zorluğu, cerebellar ataksi ve bunama gibi semptomları vardır.

Bovine Spongiform Encephalopathy (BSE): İneklerde gözüken ve CJD'nin oluşumuna neden olan formdur. İlerleyici semptomlar öncelikle davranışsal olarak sonra nörolojik olarak kendini gösterir. En önemli semptomlardan biri ışığa, dokunmaya ve sese karşı duyarlılığın ve tepkinin artması ile ataksi meydana gelir. Enfekte hayvanlar hastalığın son aşamasında ayakta duramaz hale gelirler.

Transmissible Mink Encephalopahty (TME): Faralerde görülen formudur. Önceklikle şaşkınlık, temizlik alışkanlığının kaybedilmesi, amaçsızca etrafında dönme gibi davranışsal değişiklikler gözlemlenir. Sürekli uyuklama durumu, ağırlaşma hali ve tepkisizlik hasatlığın son safhasında dikkat çeker.

Skrapi: Koyun ve keçilerde görülen paraliz ve ölümle sonuçlanan TSE formudur. Hastalığın başlangıcında aşırı telaş, sinirlilik, agresiv hareketler, sese karşı aşırı hassasiyet görülür. Kaşınma, tüy dökülmesi, uyuşukluk, düşünme ve davranışlarda belirgin yavaşlama hali,hipermetri gibi klinik bulguları en son aşamada ayağa kalkamama, pareliz, genel kas titremeleri takip eder. En yaygın TSE'lerden biri Skrapi'dir.

Skrapi ilk olarak İngiltere'de rapor edilmiş ve sonrasında Fransa, Almanya Polonya ve Avrupa'nın genelinde görülmüş sonra bütün dünyaya yayılmıştır. 2014'ün ikinci yarısında alınan raporlara göre Avrupa'da yaygın olarak bulunmaktadır.

Hastalığın ilk evrelerinde davranışsal bozukluklar gözlemlenir. Klinik bulgular hastalığın son safhasında kendini gösterdiği için hastalığın tanısı geç olmaktadır.

TSE'ler hayvanlardan insanlara geçebildiği için toplum sağlığını tehdit etmekte, hayvancılığı ise ekonomik olarak etkilemektedir. Bulaşma çevredeki uzun yıllar yaşayan etkenin alınması ile, yeme içme ile, anneden yavrusuna plasenta ile alınabilir.

Bu hastalıkları oluşturan infeksiyöz etken bakteri ya da virus değildir. Normalde hücre yüzeyinde bulunan bir proteinin yanlış katlanması ile oluşmaktadır. Yaklaşık 250 kalıntıdan oluşan bu protein PRNP adı verilen bir gen tarafından kodlanmaktadır. İlk 22 kalıntı sinyal sekansını içermektedir. Bunu şekilsiz, glisin bakımından zengin olan, Cu^{2+} bağlayan N-ucu takip etmektedir. C-ucu 121-231 rezidülerini içerir. Bu bölge düzenlidir; üç sarmal ve iki β-ipliğinden oluşmaktadır.

Doğru katlanmış protein (PrP^{c}) α-sarmal bakımından zengindir. Düzenli kısmı % 45 oranında sarmal, %3-8 β-yaprağı yapısındadır. Yanlış katlanma sonucu oluşan proteinin (PrP^{Sc}) α-sarmal içeriği azalır ve çoğunlukla β-yapraklarından (neredeyse %50 oranında) oluşur.

PrP^{c}'nin PrP^{Sc} ile karşılaşması yanlış katlanmayı katalize eder. Böylece hastalık ilerler ve hastalıklı bir canlının proteininin diğer canlıya geçmesi ile hastalık bulaşır. PrP^{Sc}'ler oligomerler ya da fibriller oluşturabilirler. Oluşan bu fibriller doku ve organlarda ölüm sonrası görülen plakları oluşturur. Beyinde ise süngerimsi boşluklu yapıların oluşmasına neden olduğu için ismi 'süngerimsi' olarak adlandırılmaktadır.

Literatür hastalık yapan bölgenin neresi olduğuna dair tartışmalıdır. Bir kısım araştırmacılar hastalığı C terminustaki yanlış katlanmadan dolayı meydana geldiğini kabul etse de N terminustaki rezidülerin yanlış katlanmasıyla oluştuğunu düşünenler de vardır. Yanlış katlanmış yapı ve buna giden yollar bilinmemektedir. Ağırlıklı olarak kabul gören kısım C terminustaki sarmal 2 (H2) ve sarmal 3'ün (H3) yanlış katlanarak β-yaprağı oluşturmasıdır. Birden fazla yanlış katlanmış yapı ve buna giden farklı yolların olması da mümkündür. Ancak yine de tam olarak yanlış katlanmış üç boyutlu yapı bilinmemekte ve bu konu araştırmaya ihtiyaç duymaktadır.

Bu çalışmada moleküler dinamik simulasyonları ile bu yanlış katlanmaya giden yolların aydınlatılmasına katkıda bulunulacaktır.

En yaygın TSE türlerinden biri olan skrapide 136, 154 ve 171. rezidülerin hastalık oluşumunda önemli olduğu bulunmaktadır. Bu çalışmada üç varyant ele alınmıştır. Bunlardan biri düşük dirençli olduğu bilinen yabanıl tiptir (ARQ: A136, R154, Q171). Diğer ikisi, en dirençsiz mutant (VRQ: V136, R154, Q171) ve en dirençli mutanttır (ARR: A136, R154, R171). Bu üç varyant birbirinden 136. ve 171. konumdaki rezidüler ile ayrılmaktadır.

Simulasyonlar Amber ff10 kuvvet alanı ve generalized Born sürekli ortam çözücü yöntemi ile 310 ve 330 K sıcaklıklarda gerçekleştrildi. Simulasyon süreleri 400 - 700 ns'dir.

310 K'deki her üç simulasyonda da proteinin hareketli bölgeleri (terminaller hariç) şunlardır: 1) Sarmal 1 ve sarmal 1 ile β-ipliği 1 arasındaki döngü (kalıntı 135-149); 2) β-iplik 2 ile α-sarmal 2 arasındaki döngü (168-177); 3) α-sarmal 2'nin C ucu ve sarmal 2 ile 3 arasındaki döngüdür (186-204). 168-177 numaralı rezidülerinin arasındaki bölgenin hareketi her üç varyantta da benzerdir.

Diğer iki bölgedeki hareketliliklerin miktarı ve yönü her üç varyantta farklı bulunmuştur. En dirençli olan ARR, diğer yapılardan daha durağandır. En dirençsiz olan VRQ'da hareketlilik en yüksektir. Dolayısıyla hareketlilik ile direnç arasında bağıntı görülmektedir. Bu varyantta özellikle sarmal 1 sarmal 3'e göre konumunu büyük oranda değiştirmektedir. Diğer iki varyantta ise kristaldeki konumundan çok uzak olmayan bir yerde kalmaktadır. Dolayısıyla sarmal 1'in hareketi 136. konumdaki valinden kaynaklandığı gözükmektedir. Diğer iki varyantta burada alanin (A) yer almaktadır.

Konformasyon değişimlerini hızlandırmak için 330 K'de yapılan ek simulasyonlarda tüm varyantlarda heliks 1'in konumunu değiştirdiği görülmüştür. VRQ'da buna ek olarak kristalde görülen beta yaprağı da bozulmuştur. Bu sonuçlar sarmal 1'in açılmasının ardından sarmal 2 ve 3'ün β-yaprağına dönüşeceğini öngören 'Banana peeling' modeli ile uyumludur.

1. INTRODUCTION

Transmissible Spongiform Encephalopathies (TSE) are fatal neurodegenerative diseases in several species including humans. Creutzfeldt–Jakob disease (CJD), fatal familial insomnia, Gerstmann- Straussler-Scheinker syndrome are TSEs observed in humans. Scrapie is found in sheep and goats, bovine spongiform encephalopathy (BSE) in cattle, transmissible mink encephalopathy (TME) in mink. TSEs in animals do not only affect the livestock, therefore the world economy, but also threaten public health by zoonotic potential from animals to human [1]. The infectious agent is not a virus or a bacterium [2]. It is a misfolded protein called prion, normally located on cell surfaces. The normally folded, "healthy" form of the prion is designated as PrP^{C}. The misfolded, "disease causing" prion form is named as PrP^{Sc}. It is known that PrP^{C} is rich of α-helical content as compared to the misfolded structure PrP^{Sc} which is rich in β-sheet content [3,4]. Contact of PrP^{Sc} with PrP^{C} triggers the misfolding of the latter. In this way, the disease propagates within the body of a patient. Similarly, the disease can pass from an individual to another if PrP^{Sc} is transferred somehow, e.g. by eating the meat of an infected animal. Whereas crystallographic structures exist for PrP^{C}, neither the structure of the misfolded protein, nor the misfolding pathway have not been obtained yet. Probably, there are many misfolded prion conformations, giving rise to different TSE diseases [5,6]. This study aims at contributing to enlighten the misfolding pathways of prions by molecular dynamic simulatons.

1.1 Transmissible Spongiform Encephalopathies in Humans and Other Animals

The most important TSEs in humans are Creutzfeldt–Jakob disease (CJD), fatal familial insomnia (FFI), Gerstmann- Straussler-Scheinker syndrome (GSS). The Creutzfeldt–Jakob disease is an incurable fatal disease which shows itself as dementia, memory loss, hallucinations and anxiety. It is the form of BSE (mad cow disease) in humans. The fatal familial insomnia has been found in 40 families in the whole world. Patients exhibit inability to sleep, rapid weight loss, hallucinations and

dementia. It eventually leads to death. The Gerstmann- Straussler-Scheinker syndrome is an extremely rare disease that starts with difficulties in speaking, then cerebellar ataxia and dementia.

Bovine spongiform encephalopathy (BSE): Cattles are effected by this form. Proggresively deteriorating symptoms which affects have firstly behavioural and then neurological effects are seen in cattles. The one noteable symptom is increasing the aggression to noise, light, touch and slowly becoming an ataxic and infected animals are unable to stand at last phase of the disease.

Transmissible mink encephalopathy (TME): TSE form which is seen in mink. Firstly characteristic behavourial changes such an confusion, loss of cleanliness and aimless circling are observed in mice. Drowsiness and unresponsiveness are seen at last phase of the disease

Scrapie is a form of TSE in sheep and goats that results in paralysis and death. At the beginning, mainly behavioral signs are seen such as increased excitability, nervousness, aggressiveness, increased sensitivity to noise. Clinical signs show themselves at the terminal state: pruritus, rubbing, hypokinesis, hypermetria followed by falling, general paresis, tremors, muscle fasciculations.

1.2 Search for the Cause of TSEs

The transmission of the disease could arise in three different ways: acquired, familial or sporadic way [7].

The infection agent is able to persist for a long time in soil [8, 9]. Therefore, infection could be by the environmental way [10]. Also agents can infect humans by oral way [11, 12]. Researches about prion diseases increased after the observation that BSE could be transmitted to human when contaminated meats are consumed, causing variant Creutzfeldt-Jakob disease (vCJD). This is the acquired way of the disease [13].

A gene which is prone to cause disease transmitted by genetically to next generation. This is the familial way of the disease[14].

Somatic mutation or spontaneous transformation of PrP^{c} to PrP^{Sc} cause to form sporadic way of the disease[15].

Agent of the scrapie was first considered to be an atypical virus belonging to the slow virus group [16]. Later studies by Alper et al. and Prusiner dismissed the viral theory [17]. Prusiner developed a new theory known as 'the protein only hypothesis', and suggested that the scrapie agent is a pathogenic protein with infectious features, that he called a prion 'PrP^{Sc}' [2, 18]. This protein consists of β-sheets and gives rise to prion fibrils upon oligomerization.

Prusiner's theory is based on the observations below:

- PrP^{Sc} and scrapie infectivity copurify when biochemical and immunologic procedures are used.
- The unusual properties of PrP^{Sc} mimic those of prions. Many different procedures that modify or hydrolyze PrP^{Sc} inactivate prions.
- Levels of PrP^{Sc} are directly proportional to prion titers.
- No evidence exists for a virus-like particle or a nucleic acid genome.
- Accumulation of PrP^{Sc} is invariably associated with the pathology of prion diseases, including PrP amyloid plaques that are pathognomonic.
- PrP gene mutations are genetically linked to inherited prion disease and cause formation of PrP^{Sc}.
- PrP^{Sc} preferentially binds to homologous PrP^{C}, resulting in formation of nascent PrP^{Sc} and prion infectivity.

1.3 Prions

PrP^{C} is thought to be a post-translationally modified form of the host-encoded membrane glycoprotein which is encoded by PRNP gene. Prion proteins include approximately 250 residues. The first 22 residues constitute a signal sequence, followed by an unstructured, Cu^{2+} binding N-terminal region that contains octarepeats rich in glycine [2]. The C-terminal region of PrP spans residues 121-231 and is ordered, consisting of three helices (H1,H2,H3) and two short β-strands (β1, β2) [19]. H2 and H3 are connected through a disulfide bridge [20]. The structure of the ordered C-terminal region of PrP^{C} was elucidated by using crystallography and nuclear magnetic resonance (NMR) methods. The structure of the C-terminal region

of the sheep prion protein is given in Figure 1.1. Several mammalian prion proteins show high sequence identity.

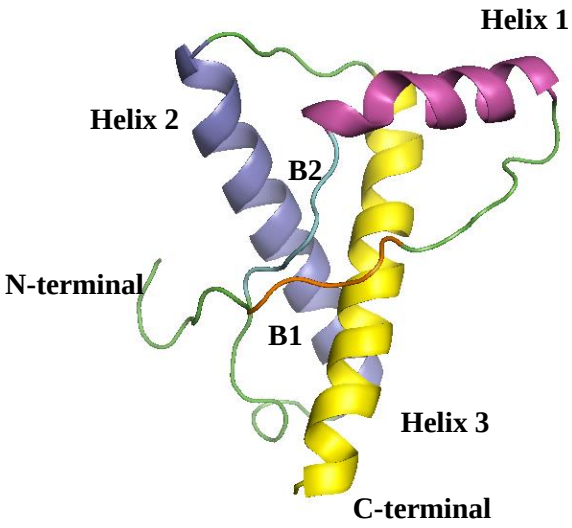

Figure 1.1 : Crystallographic structure of the C-terminal part of PrPC

An abnormal isoform of PrP^{C} is PrP^{Sc} which is the infectious agent responsible for TSE diseases [21]. Although PrP^{C} and PrP^{Sc} have the same amino acid sequence [22], the physical characteristics of PrP^{Sc} are profoundly different than those of PrP^{C} [21]. PrP^{Sc} has diminished α-helical content and is rich of β-sheets compared to PrP^{C} [3,4]. The ordered region of PrP^{C} (residues 121-131) is 45% helical with a very low (3–8%) β-sheet content [23, 24]. On the other hand, the secondary structure of PrP^{Sc} has approximately 50% β-sheet content according to Fourier transform infrared spectroscopy [25, 26]. The high β-sheet content of PrP^{Sc} makes it partially resistant to protease digestion.

Spontaneous transition of PrP^{C} to PrP^{Sc} is slow. However, once formed, PrP^{Sc} can act as a template for the accelerated conversion of another PrP^{C} to PrP^{Sc}. PrP^{Sc} forms aggregates that can build fibrillar filaments, and finally forms the fatal plaque deposits which are found postmortem in organs and tissues. Fractionation of fibrils provides new seeds for further PrP^{C} to PrP^{Sc} conversion. This mechanism is depicted in Figure 1.2.

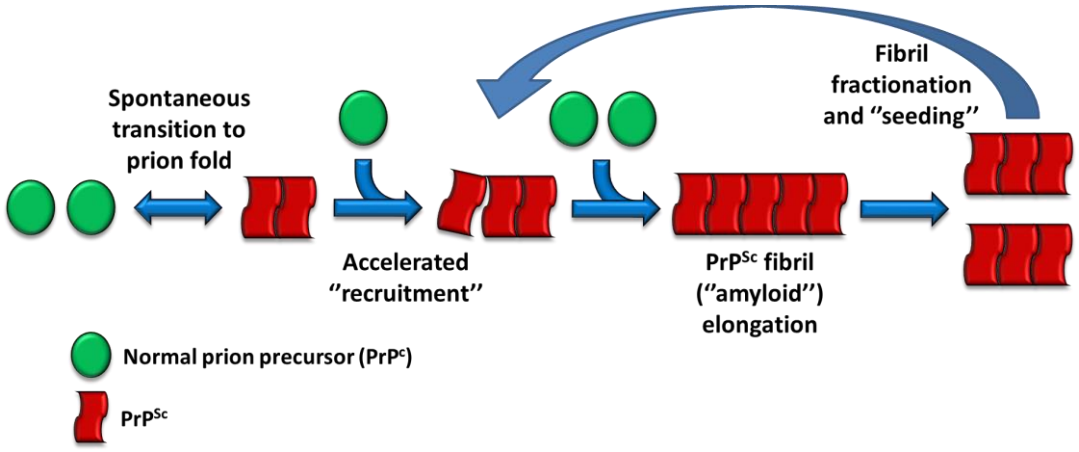

Figure 1.2 : Spontaneous transition to prion fold mechanism.

Brain tissue is affected by the formation of these filaments and it is seen like a sponge with tiny holes (Figure 1.3).

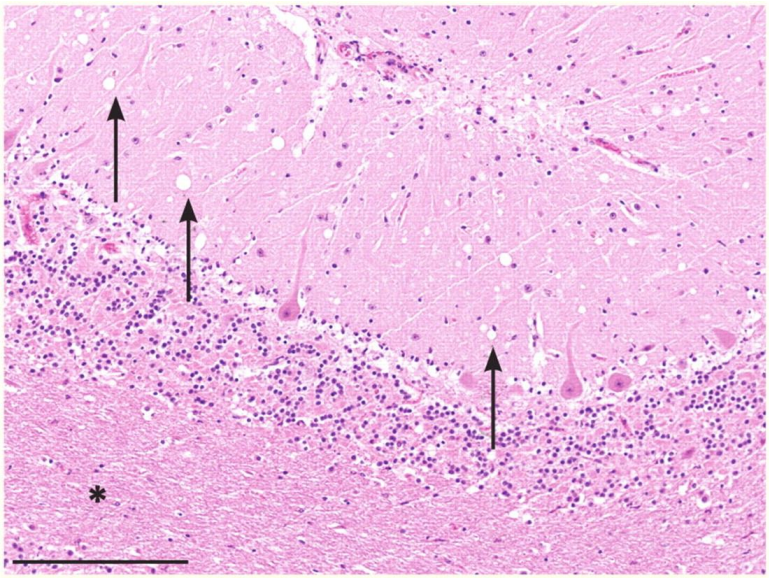

Figure 1.3 : Cerebellum of a sheep with atypical scrapie, vacuolizations of neurons.

1.4 MD Simulations in Literature

Some researchers believe that β-rich core of the scrapie isoform comprises last part of N-terminal tail and C-terminal tail which is up to H1 [27]. A common view suggests the B1H1B2 region is crucial for sheet seeding and PrP^{Sc} formation [28,29]. H1 has been implicated as a primary interaction site between PrP^{Sc} and PrP^{C} [2,30]. whereas the loop between B2 and H2, a rigid loop stabilized by its long range interactions with H3 [48], and the C-terminus of H3 has been suggested to be recognized by a "Protein-X" that would affect the conversion of PrP^{C} into PrP^{Sc} [49].

One of the study high level of β-structures are observed when C-terminal part (residues 124-226) of the molecule performed in a replica exchange molecular dynamic simluations (REMDs) during 2,8 μs in mouse prion protein. 10 different β-rich folds are defined according to their topology, accumulation temperatures and strucrutal characteristics [27] (Figure 1.4).

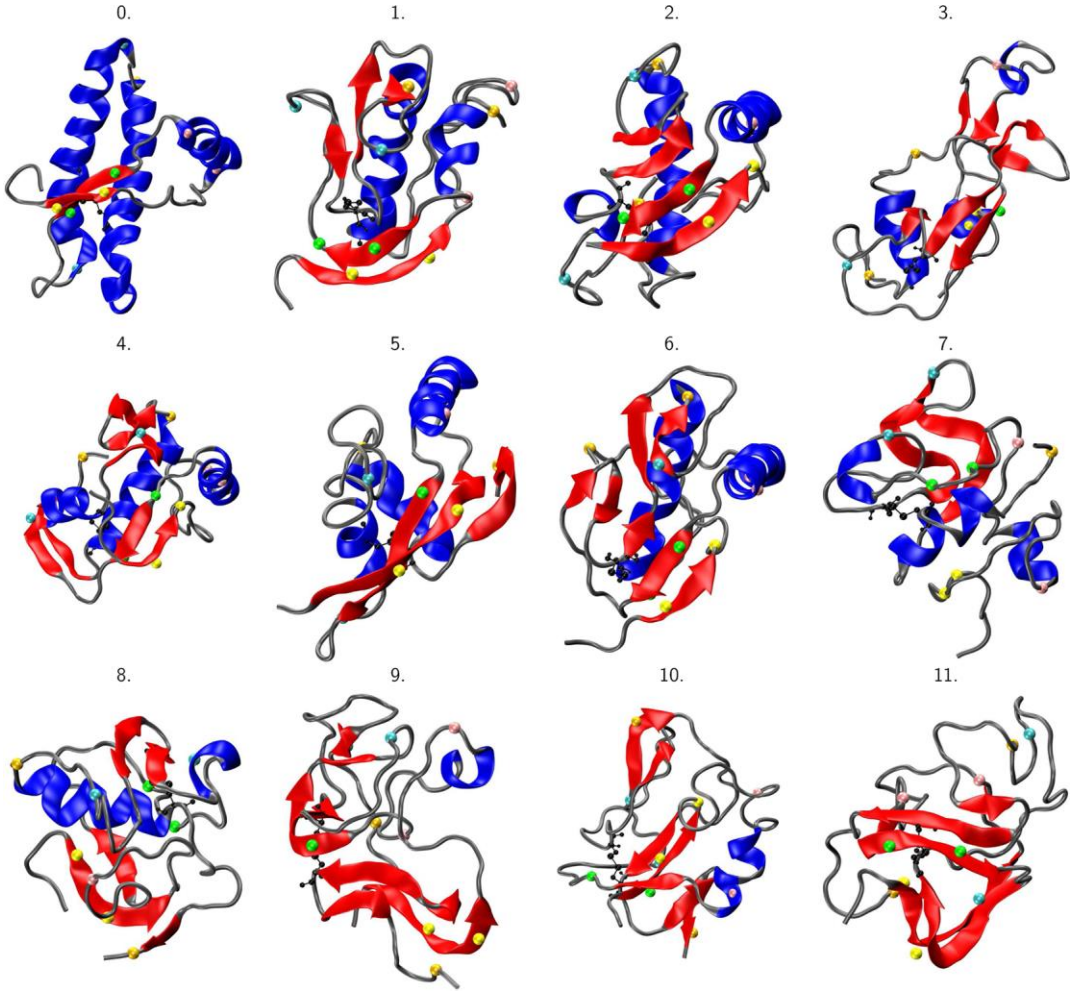

Figure 1.4 : β-rich folds . Panel 0 shows NMR structure, Panel 11 shows the maximal β-content structure obtained in simulation [27].

The mutation has performed A117V in order to investigate the impacts of A117V on prion diseases at another study. They observed that A117V mutation increases the sheet contents and aggregation propensity via inter-peptide backbone hydrogen bonding interactions and side chain hydrophobic interactions [33].

One of the study human prion protein has simulated at pH 2 and pH 7, respectively. It is believed that PrPC do not undergo misfolding at neutral pH. Low pH levels are important to conversion of PrPC to PrPSc. Increasing the temperature 310K, 350K

and 450K respectively for pH7 and pH2 simulations. Obtained structures are very different from the starting structure. They believe that under native conditions the stabilization energy is concentrated in regions of the H1 and H3. Misfolding starts with a spreading of the stabilization energy over H2, which destroys the native stabilizing core [34]. The other experiment observed reversibility of the misfolding of the prion protein on their short constant-pH molecular dynamic simulations. They started simulations as pH7 then expose pH2. They observed that pH-induced misfolding of PrP [35].

Also different studied had perfomed in order to understand the effect of electro-static potential. The experiment which is performed on rabbit prion protein shows that there is a large land of surface positive electrostatic charge distributions for $RaPrP^{C}$ wild type during long MD simulations although mutants are not able to show [36].

Molecular dynamics simulation performed on H187 in non-mammalian species that are known to be resistant to prion diseases. They observed two different misfolding routes upon the protoneation H187. Imidazole ring of H187 is protonated. It is seen that this residue experiences an electronic repulsion with guanidinium group of R136 and displayed different misfolding route [37].

Also another study simulated mouse prion protein during 680ns in order to inspect dynamics of the helical fragments. They believe that H1 formation is stabilized by internal salt bridge. Some mutations on H1 (D147A, R151A) alter the helix macrodipole which is required. Therefore this conformational change is unlikely in the PrP^{C} to PrP^{C*} transition. The second half of H2 and H3 undergo transition from α-helical conformation to β-sheet [38]. This study is also similar with a study which refer 'banana peeling' model. According to 'banana peeling model' H1 (banana skin) should be removed in order to expose H2 and H3 to promote conversion from a helical to β-rich structure.

1.5 Aim of This Study

TSE (Transmissible Spongiform Encephalopathies) are fatal, progressive neurodegenerative diseases. Misfolding pathways of prion proteins leading to TSE

diseases should be elucidated for both human-community health care and livestock farming and economy.

The aim of this study is to contribute to the understanding of the PrP^{C} to PrP^{Sc} transformation which causes the TSE diseases. To this aim, molecular dynamics (MD) simulations on the wild type and two mutant prion proteins have been performed.

Scrapie is one of the most common TSE diseases of livestock in the world. The residues at positions 136, 154 and 171 have important roles in determining the susceptibility to scrapie [39]. The variant with V136, R154, Q171 displays a high susceptibility whereas the variant with A136, R154, R171 has a high resistance. The variant with A136, R154, Q171 has a low resistance. In this work, these sequences are denoted as VRQ, ARR and ARQ, respectively. In the literature, the ARQ sequence is considered to be the wild type [39]. Therefore, we have selected the wild type sequence together with the most resistant (ARR) and least resistant (VRQ) sequences of sheep prion for the MD simulations. The results of these simulations have been compared in order to understand the roles of the residues at positions 136 and 171 in the misfolding process. We have also carried out additional simulations at 330K in order to accelerate conformation changes and inspect more conformations.

2. METHODOLOGY

Molecular Dynamics (MD) simulations can be applied in the investigation of a wide range of dynamic properties and processes by researchers in numerous fields, including structural biochemistry, biophysics, enzymology, molecular biology, pharmaceutical chemistry, and biotechnology. Simulations can provide the ultimate detail concerning individual particle motions as a function of time. Thus, they can be used to address specific questions about the properties of a model system, i.e. specific aspects of biomolecules, kinetics and thermodynamics, often more easily than experiments on the actual system. Furthermore, a variety of studies including drug design and protein design, structural determination and refinement can be performed via MD. Experiments play essential role in validating the simulation methodology: comparisons of simulation and experimental data serve to test the accuracy of the calculated results and to provide criteria for improving the methodology [40]. Recently, molecular dynamics simulations have been widely used to test the structure, dynamics and thermodynamics of biological molecules as well as for the determination of structures from X-ray crystallography and from NMR experiments.

2.1 Force Fields

In the context of molecular mechanics, a force field refers to the functional form and parameter sets used to describe the potential energy of a system of particles (typically but not necessarily atoms). Force field functions and parameter sets are derived from both experimental work and high-level quantum mechanical calculations. A force field is mainly composed of two parts: bonded terms and non-bonded terms. Bond stretching, angle bending and torsion angle can be taken into bonded terms, similarly, van der Waals and Coulomb forces can be taken into non-bonded terms contributions (Figure 2.1).

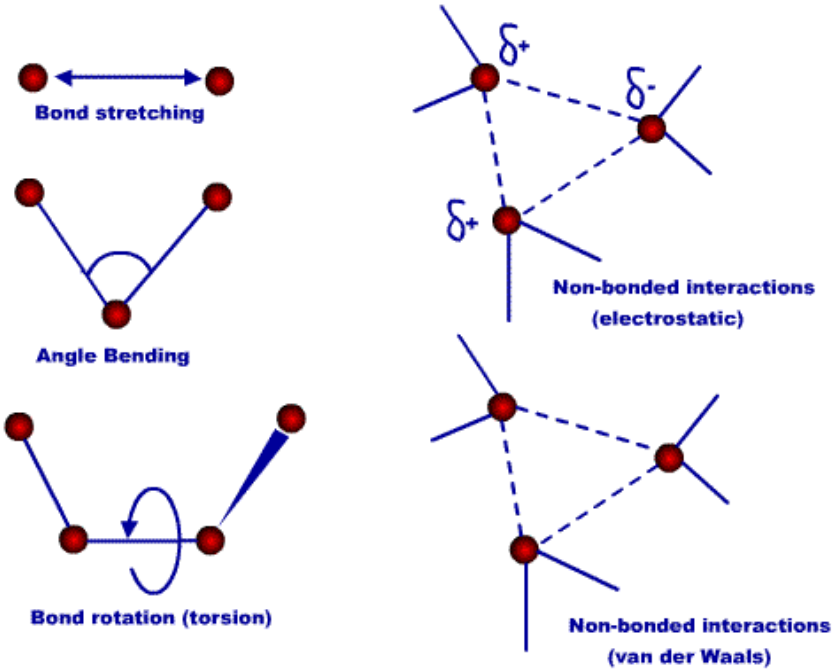

Figure 2.1 : Force field contributors.

By using these contributions to the potential energy, E, can be evaluated as the following:

$$E = E_b + E_s + E_\omega + E_{nb} \qquad \textbf{(2.1)}$$

E_s is the energy for bond stretching, E_b is the energy for bond angle bending, Eω is the torsional energy due to twisting about bonds and E_{nb} is the energy for non-bonded interactions. Many different kinds of force-fields have been developed over the years. Some include additional energy terms that describe other kinds of deformations. Some force-fields account for coupling between bending and stretching in adjacent bonds in order to improve the accuracy of the mechanical model. The design of force-fields for molecular mechanics is guided by the following principles:

i) Nuclei and electrons are lumped into atom-like particles.

ii) Atom-like particles are spherical (radii obtained from measurements or theory) and have a partial charge (obtained from theory).

iii) Interactions are based on springs and classical potentials.

iv) Interactions parameters must be preassigned to specific sets of atoms types.

v) Interactions determine the spatial distribution of atom-like particles and their energies.

2.1.1 Stretching and bending

Considering the idea of a molecule to be a collection of masses connected by springs, by applying Hooke's Law we can evaluate the energy required to stretch and bend bonds from their ideal values. Thus E_s and E_b may be expressed as:

$$E_s = \sum_{i=1}^{N} \frac{k_i^s}{2}(l - l_0)^2 \quad \textbf{(2.2)}$$

$$E_b = \sum_{i}^{M} \frac{k_i^b}{2}(\theta - \theta_0)^2 \quad \textbf{(2.3)}$$

where N is the total number of bonds and M is the total number of bond angles in the molecule. k^s and k^b are the force constants for stretching and bending respectively. l and θ are the actual bond lengths and bond angles. Finally l_0 and θ_0 are ideal bond lengths and bond angles. Unique k^s and l_0 values are assigned to each pair of bonded atoms based on their types (e.g. C-C, C-H, O-C, etc.). Similarly k^b and θ_0 parameters for angle bending are assigned to each bonded triplet of atoms based on their types (e.g. C-C-C, C-O-C, C-C-H, etc.).

2.1.2 Torsion

We consider the form of the Eω term. The energy due to torsion is usually expressed in terms of a Fourier series,

$$E_\omega = \sum \frac{V_n}{2}(1 + \cos[n\phi - \gamma]) \quad \textbf{(2.4)}$$

where the sum is over all unique sequences of bonded atoms. ω is the torsion angle and γ is the phase factor.

2.1.3 Non-bonded interactions

The final term contributing to E is the energy from pairwise non-bonded interactions. These interactions are van der Waals forces and electrostatic interactions.

$$E_{non-bonded} = \sum_i \sum_{j>1} \left(\frac{A_{ij}}{r_{ij}^{12}} - \frac{B_{ij}}{r_{ij}^{6}} \right) + \sum_i \sum_{j>1} \frac{q_i q_j}{\varepsilon r_{ij}} \qquad \textbf{(2.5)}$$

where, van der Waals interaction between two atoms i and j separated by distance rij is described by Lenard Jones potential with parameters A_{ij} and B_{ij}, and a Coulomb potential describes the electrostatic interaction between a pair of atoms i and j using qi and qj as partial charges on the atoms and ε as the dielectric constant of medium.

Usually the parameters for the non-bonded energy terms are obtained by measuring non-bonded contact distances in crystalline hydrocarbons, diamond, graphite and van der Waals contact data for rare gas atoms. Parameters for other atoms are then obtained by extrapolation or interpolation. One major assumption is that the potential derived from intermolecular interactions can accurately reproduce intramolecular interactions. In addition the interactions are considered to be pairwise additive [41].

An important non-bonded energy term that is always taken into account is the electrostatic interactions. Typically the electrostatic interaction dominates the total energy of a system by a full magnitude. The electrostatic contribution is modeled using a Coulombic potential.

The electrostatic energy is a function of the charge on the non-bonded atoms, their interatomic distance, and a molecular dielectric expression that accounts for the decrease of electrostatic interaction due to the environment (such as by solvent or the molecule itself). A linearly varying distance-dependent dielectric (i.e. 1=r) is sometimes used to account for the increase of ε in environmental bulk as the separation distance between interacting atoms increases. The accuracy of the electrostatic term depends on the correct assignment of charges to individual atoms.

The terms describing energy changes from bond length, bond angle and torsions are well understood and can be accurately included in the overall energy expression. The most influential term, the electrostatic term, however is not fully understood. Hence the variation in results from different force fields can be attributed, to a large extent,

to the electrostatic term. Of course the nature of the parameterizations generating the various force constants and ideal lengths and angles will also affect the applicability of a force field. In general one must consider with which group of molecules or systems a given force field has been parameterized – keeping this fact in mind one may then use the force field on an unknown but similar system. Generality is still a problem with force fields, though with the development of the Universal Force Field (UFF) [42] an attempt has been made to develop a generalized force field applicable to a large portion of the periodic table and not be restricted to particular groupings of atoms such as proteins, nucleic acids etc.

2.2 Theory of Molecular Dynamics

The state of any classical system can be completely described by means of specifying the positions and momentum of all particles:

$$\begin{aligned} \mathrm{q} &= (x_1, y_1, z_1, x_2, y_2, z_2, \ldots) \\ \mathrm{p} &= (\mathrm{p}_{x,1}, \mathrm{p}_{y,1}, \mathrm{p}_{z,1}, \mathrm{p}_{x,2}, \mathrm{p}_{y,2}, \mathrm{p}_{z,2}, \ldots) \end{aligned} \tag{2.6}$$

Since a phase point is defined by the positions and momentum of all particles, it determines the location of the next phase point in the absence of outside forces acting upon the system. Therefore, the relationship between two positions in any time interval is given by:

$$q(t_2) = q(t_1) + \int_{t_1}^{t_2} \frac{p(t)}{m}\, dt \tag{2.7}$$

where;

$$v = \frac{p}{m} \tag{2.8}$$

Similarly, the relationship between any two momentum vectors is:

$$p(t_2) = p(t_1) + m\int_{t_1}^{t_2} a(t)dt \quad \textbf{(2.9)}$$

using Newton‟s Second Law of Motion:

$$a = \frac{F}{m} \quad \textbf{(2.10)}$$

Moreover, the average value of any property during this time evolution is:

$$\langle A \rangle = \frac{1}{M}\sum_i^B A(t_i) \quad \textbf{(2.11)}$$

where B is the number of times the property is sampled. Sampling continuously and following the trajectory indefinitely, this equation becomes:

$$\langle A \rangle = \lim_{t\to\infty} \frac{1}{t}\int_{t_0}^{t_0+t} A(t)dt \quad \textbf{(2.12)}$$

assuming ergodic hypothesis to be valid and independent of choice of t0 [47].

2.3 Simulation Parameters

In this study, all calculations have been carried out using the Amber 14 program package [43,44]. The ff10 force field (which is equivalent to ff99SB for proteins) has been used.

We have taken three different protein strains with PDB (protein data bank) codes 1TQB, 1TQC and 1TPX. These structures correspond to variants V136, R154, Q171 (VRQ); A136, R154, R171 (ARR) and A136, R154, Q171 (ARQ), respectively. These proteins were co-crystalized with antibodies. Therefore we have removed antibodies from crystallographic structures. Similarly, water molecules have been deleted because an implicit solvent model is used. Disulfide bonds have been formed between cysteines located at positions 182 and 217 in all protein strains. These

structures lack the N-terminal part of the proteins and start at G127. Experimentally, the N-terminal region is known to have no important effect on the formation of PrP^{Sc}. Therefore this region has not been included in these simulations. Only the C-terminal parts (G127-P223) of all three proteins have been simulated.

Propka server has been used to predict the pKa values of ionizable residues. Protonation states have been assigned assuming a neutral pH (pH = 7). In addition, visual inspection of crystal structures has provided insight about the protonation states. All aspartates, glutamates and lysines have been taken in their ionized states. The protonation states of histidines are as follows:

- Residue H143 as HID.
- Residue H180 as HIE.
- Residue H190 as HIE.

Generalized Born (GB) solvation model has been used to take into account the solvent effects implicitly [45]. We have been used gb=5 which is developed by A. Onufriev, D. Bashford and D.A. Case corresponds to model II [46]. The solute protein has been put in a cavity in a continuum represented by its dielectric constant (ε = 78.4 for water). The cavity has been generated by using the mbondi2 atomic radii. A 0.1 molar salt concentration has been used. A cut off value of 30 Å has been used to truncate the van der Waals and electrostatic interactions. Electrostatic and van der Waals interactions between atoms that are separated by more than 30 Å have been completely neglected.

All structures have been minimized until the root mean square gradient is less than 0.01 kcal/mol.Å. The first NCYC 500 steps have been made by using the steepest descent algorithm, whereas in the rest of the minimization the conjugate gradient algorithm has been employed.

The computations have been performed by constraining hydrogen - heavy atom stretching motions using the SHAKE algorithm, allowing a time step of 2 fs. All three structures have been simulated at both 310 and 330 K. Simulations have been started at 10K and heated to 310 K or 330 K. The temperature has been adjusted by using a Langevin thermostat.

Some regions in the VRQ simulation displayed a tendency to form β-sheets. Distance restrains have been imposed to some backbone N and O atoms in these regions in order to force the formation of β-sheets. Two snapshots have been selected from the VRQ simulation. In one of them, the distances between G198-N and T194-O, G198-O and T194-N, N200-N and V192-O have been restrained. In the other one, the distances between T194-N and R159-O, T194-O and R159-N have been restrained.

For cluster analysis, cluster radii of 4 Å have been used for simulations at 310 K.

3. RESULTS AND DISCUSSIONS

Simulations have been carried out for the most resistant variant ARR (A136, R154, R171) for 600 ns, and the low resistant variant ARQ (A136, R154, Q171) for 400ns. The variant VRQ (V136, R154, Q171) which is the most susceptible form has been simulated for 700 ns at 310 K.

Results are given in the following sections. First, studies performed at 310 K are discussed, then these studies are compared with studies performed at 330 K

3.1 Simulations at 310K

3.1.1 Stability of simulations at 310 K as displayed by the root mean square deviations (RMSD)

The evolution of the RMSD values with respect to the initial structure is an indication of the stability of the structures. The RMSD values for ARR, ARQ and VRQ are given in Figure 3.1 , Figure 3.2 and Figure 3.3 respectively.

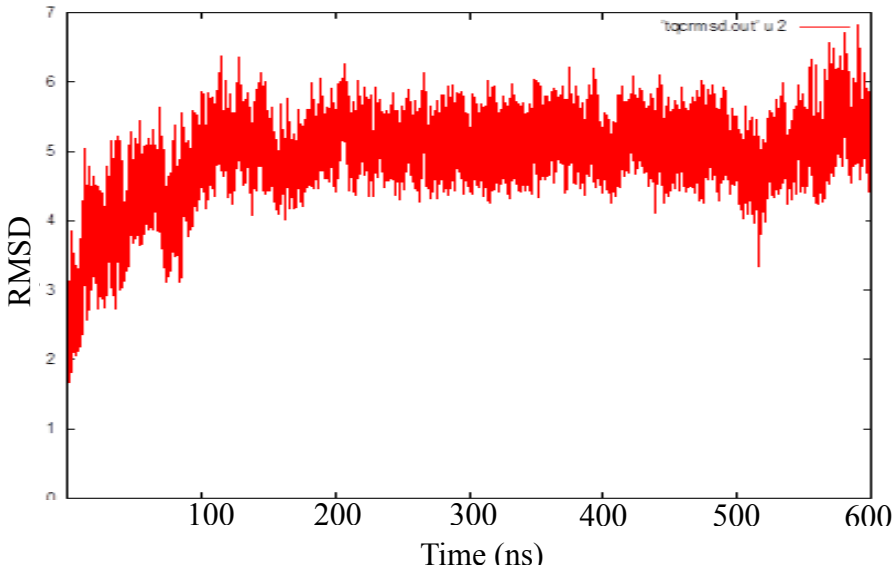

Figure 3.1 : RMSD with respect to time for ARR at 310 K.

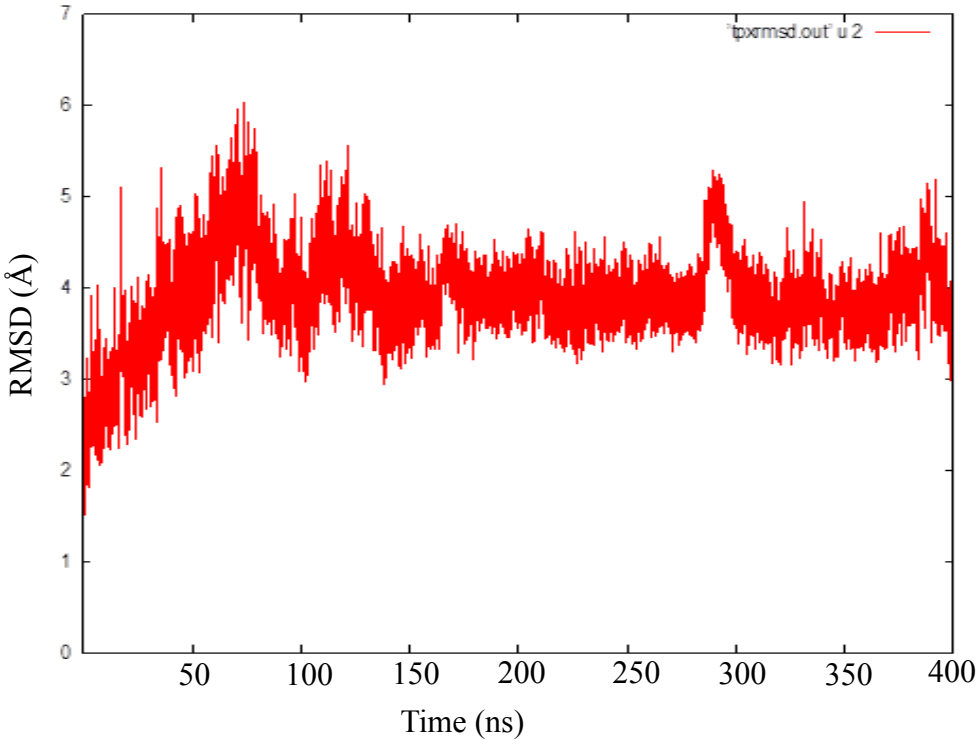

Figure 3.2 : RMSD with respect to time for ARQ at 310 K.

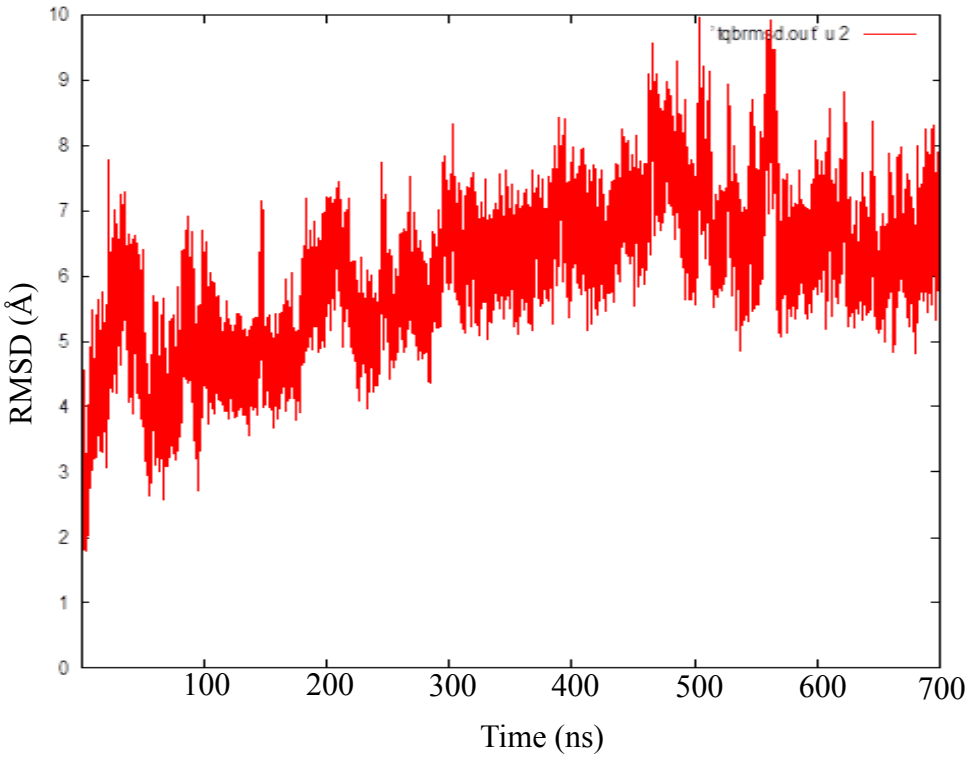

Figure 3.3 : RMSD with respect to time for VRQ at 310 K.

In all three simulations there is a noteable increase in RMSD values within the first 100 ns. The increase by 5Å, 4Å and 6Å for ARR, ARQ, VRQ are shown respectively in Figure 3.1 Figure 3.2 and Figure 3.3. Therefore this part could be considered as equilibration period of these simulations.

During the remaining part of the ARR and ARQ simulations, the RMSD values are relatively stable with only small deviations. However, the RMSD values of VRQ oscillates along the simulation. After first 200-250 ns some more conformational changes take place.

These interesting results show that significant conformational changes take place throughout the whole VRQ simulation whereas the other two simulations (ARR, ARQ) are quite stable after the equilibration period. This behavior correlates with the scrapie susceptibility among these variants.

The most susceptible structure exhibits continuous oscillations throughout the simulation whereas less susceptible variants acquire stable structures. The reason for these oscillations will be described below.

3.1.2 Mobility of the residues

B-factor indicates the true static or dynamic mobility of an atom. In order to identify the regions of the proteins with high fluctuations, the B-factor values of ARR, ARQ, VRQ have been computed and displayed respectively in Figure 3.4, Figure 3.5, Figure 3.6. Regions with high mobility are shown in Figure 3.7.

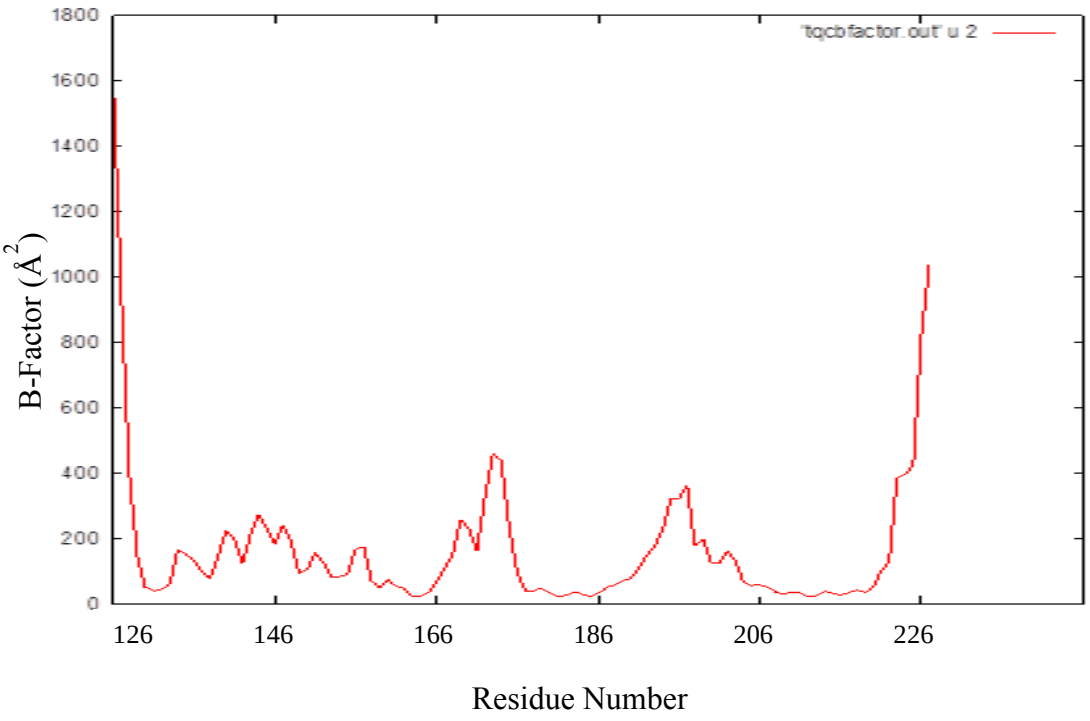

Figure 3.4 : B-factors (Å^2) in the ARR simulation at 310 K

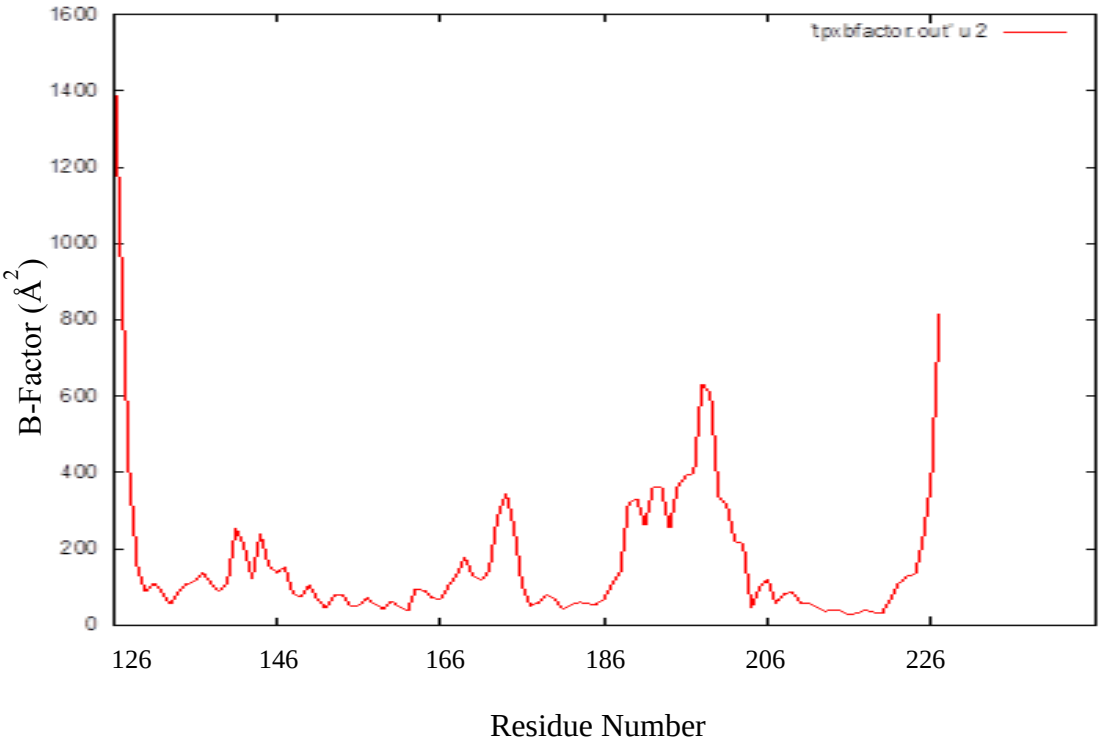

Figure 3.5 : B-factors (A^2) in the ARQ simulation at 310 K.

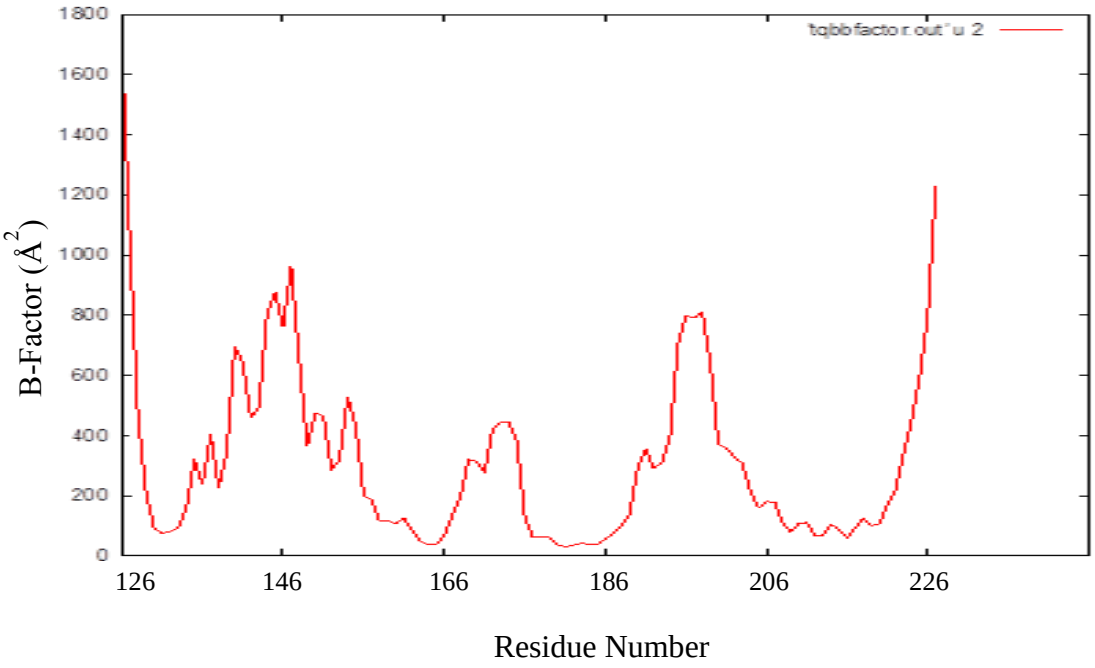

Figure 3.6 : B-factors (Å^2) in the VRQ simulation at 310 K.

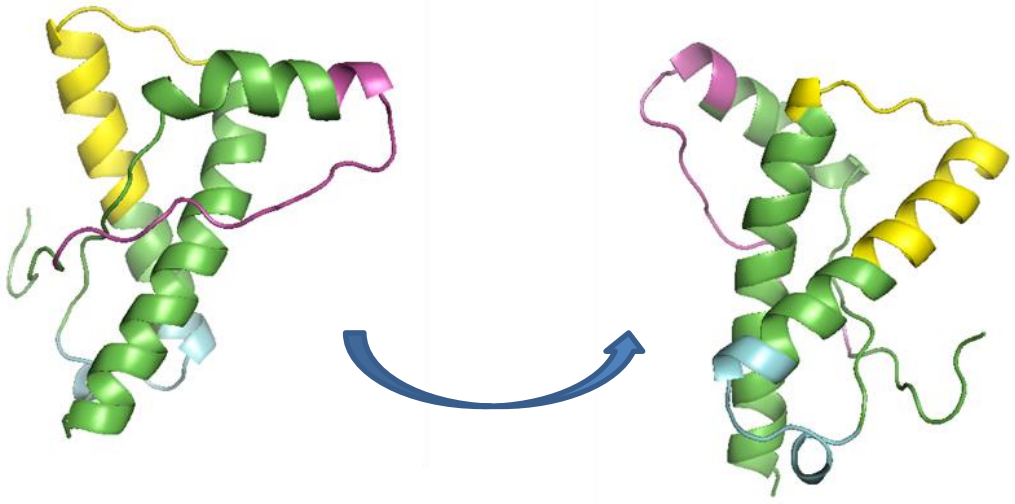

Figure 3.7 : Residues with high mobility. Pink: residues 135-149; blue: residues 168-177; yellow: residues 186-204.

The N terminus and C terminus generally show high mobility in all simulations. These termini are not involved in strong interactions with the rest of the protein. Therefore their high mobility is expected and not significant for understanding the difference between variants considered in this study.

The other highly fluctuating residues are divided into three groups: Residues 135-149, 168-177 and 186-204. No difference has been observed at the position and the dynamics of R/Q171 during simulations as mentioned section 3.2.1.

The computationally observed relation of the mobility and susceptibility of Q/R may be due to coincidence. The fluctuations of residues 168-177 are very similar in all simulations. On the other hand the magnitude of B-factors in the region 186-204 is in the order VRQ > ARQ > ARR. This order corresponds to the order of susceptibility to scrapie. However the sequence in this region is identical for all three variants. Therefore the polymorphism at positions 136(V/A) and 171(R/Q) may have indirect effects on the region 186-204. This point needs to be clarified by further studies. This region contains the C terminal part of helix 2 and the loop connecting helix 2 to helix3. This sequence is rich in threonine which provide a high flexibility. As a result the C terminus of helix 2 unfolds and refolds continuously during the simulations. Representative conformations are given in Figure 3.8

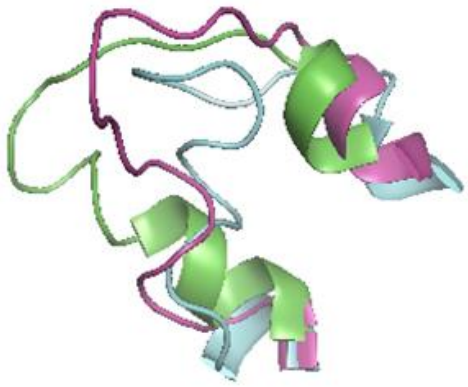

Figure 3.8 : C terminal part of H2 and the loop connecting H2 to H3 where rich in threonine shows high flexibility.

Residues 135-149 do not fluctuate as much as the other residues in ARR and ARQ simulations while they constitute most mobile region in VRQ simulation with a considerable peak as shown in the figure 3.6. This region corresponds to H1 and the loop connecting β-strand 1 to H1, and contains A10/V10. High fluctuation exhibited by VRQ can be related to the presence of V10 and can result with its high scrapie susceptibility. The effect of the V10 will be discussed in the following sections.

3.1.3 Cluster analysis

By using a radius of 4 Å in cluster analysis for ARR, ARQ, VRQ, 3, 3 and 18 clusters have been obtained, respectively. H1 mobility in ARR is not seen significantly and clusters are displayed in Figure 3.9 and Figure 3.11

In ARR, a new 3_{10} helix (one turn long) forms between β-strand 1 and H1 and it remains stable during the whole simulation (Figure 3.10). It is the characteristic of the most populated cluster (cluster 0). The C-terminus of H2 and the loop between H2 and H3 have also some mobility and the C-terminus of H2 loses its α-helical conformation, although very rarely (cluster2). But these changes which are located in H2 are not as pronounced as those in the β-strand 1 and H1 (Figure 3.9, Figure 3.10).

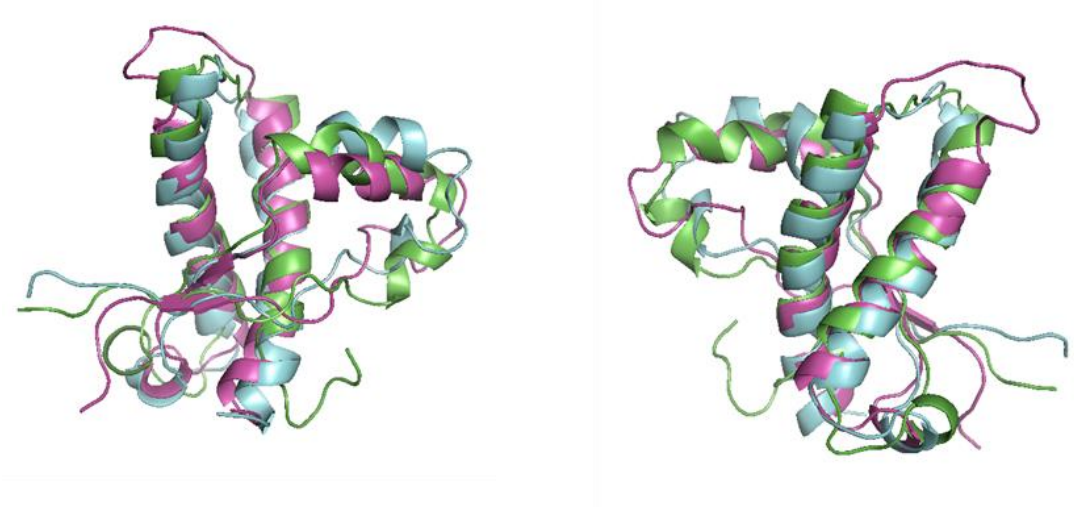

Figure 3.9 : Clusters of ARR using a 4 Å radius (green: cluster 0, blue: cluster1, pink: cluster2).

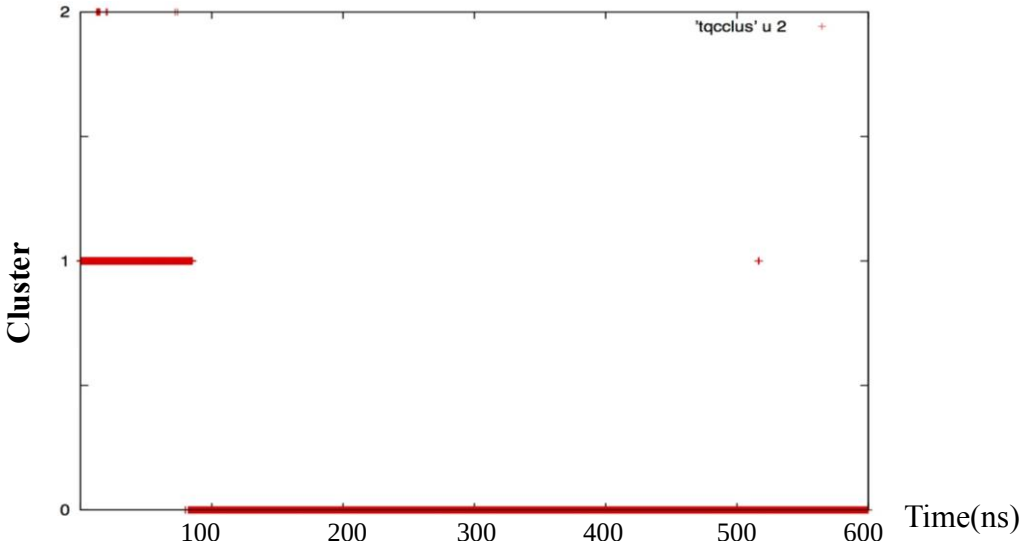

Figure 3.10 : Clusters and cluster members of ARR with respect to time.

H1 mobility is seen rarely in clusters of ARQ. Also, the magnitude of the movement is low as seen in the B-factor graphs. There is no formation of α-helix between β-strand 1 and H1, unlike ARR. The fluctuations are observed mostly at the C-terminus of H2 and the loop between H2 to H3. The C-terminus of H2 loses its α-helical

structure in the most populated cluster (cluster 0 in Figures 3.11 and 3.12). On the other hand, H2 is stable in the second most populated cluster (cluster 1). The time evolution of the clusters is seen in Figure 3.12.

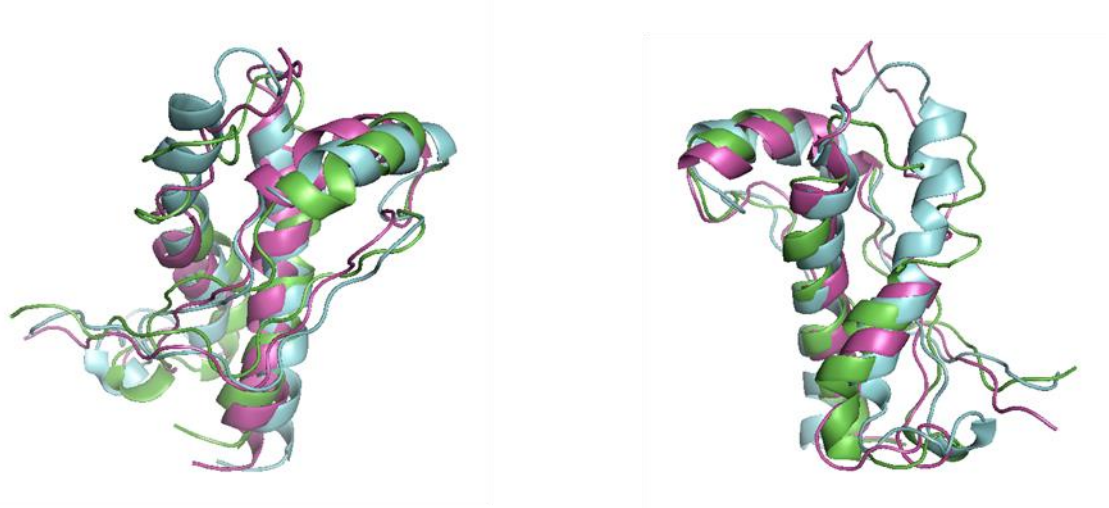

Figure 3.11 : Clusters of ARQ using 4 Å radius (green: cluster 0, blue: cluster1, pink: cluster2)

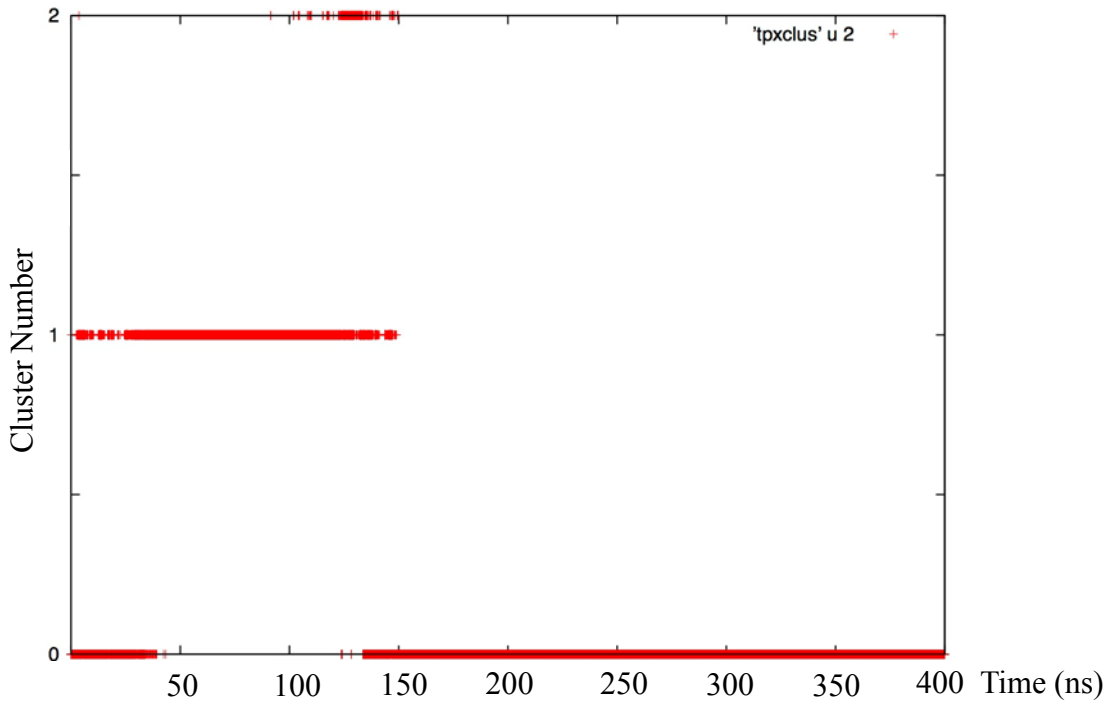

Figure 3.12 : Clusters and cluster members of ARQ with respect to time.

Different cluster formations are observed in VRQ simulations showing that the stability of VRQ is lower than the others (ARR, ARQ). We have obtained 18 different clusters by using a 4 Å cluster radius (Figure 3.13). Most of the fluctuations take place in H1. Also B-Factor figure shows that conformational changes in H1 are

unique for VRQ when it is compared with the ARR and ARQ. H1 rotates away from H3 or move towards the C terminus of H3 as displayed in Figure 3.14.

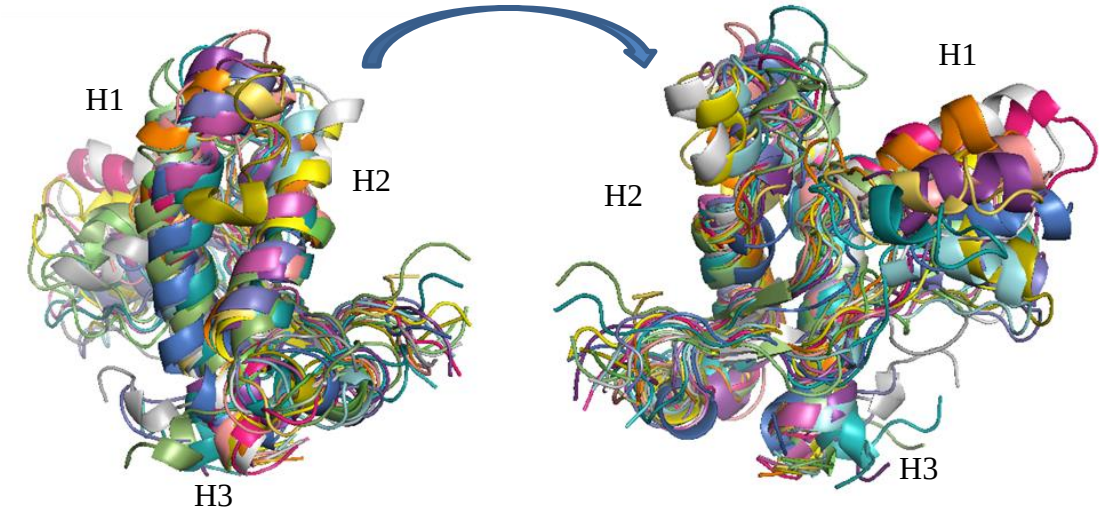

Figure 3.13 : Clusters of VRQ using 4 Å radius.

Figure 3.14 : Green: similar to crystal position (cluster 3); Pink: H1 rotates away from H3 (cluster 10) ; Purple: H1 move towards the C terminus (cluster 6).

In addition to the motion of H1, residues 186-204 adopt very different conformations. In some of them the C-terminal part of H2 is unfolded.

In clusters 3 and 5, the position of H1 is similar to that in the crystal structure. H1 has moved towards the C-terminus in clusters 1, 2 and 6, while in clusters 4 and 7, 10 H1 rotates away from H3. The time evolution of the clusters is depicted in Figures 3.15 and 3.16 (clusters with low populations are omitted).

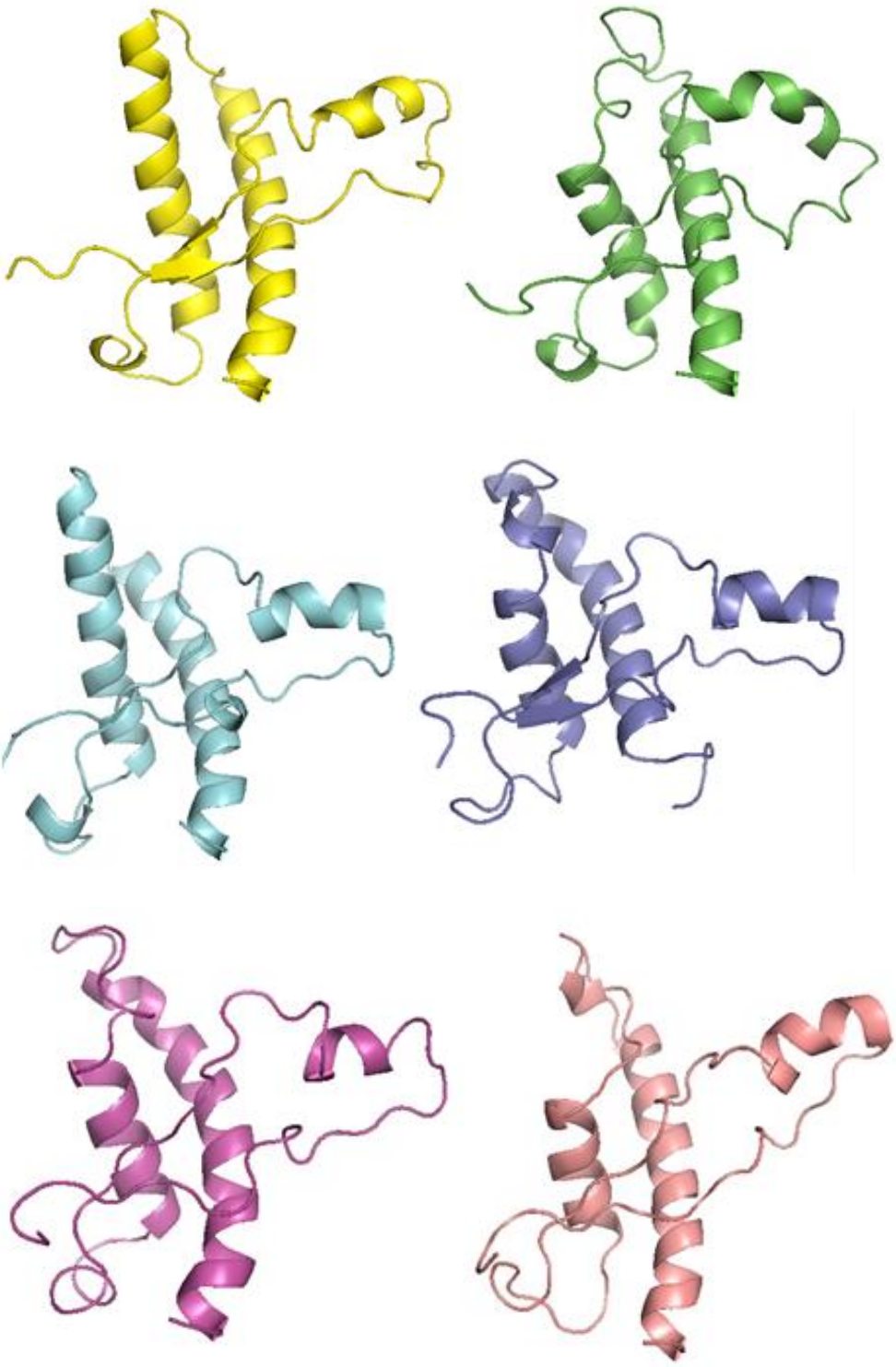

Figure 3.15 : Time evolution of the position of H1 in VRQ simulation. (Yellow: cluster 3; Green: cluster 0; Cyan: cluster 1; Purple: cluster 6; Pink: cluster 2; Salmon: cluster4.)

As can be seen from Figure 3.15, repositioning of H1 is not a permanent change. H1 explores three different positions (Figure 3.16). Conspicuous 3_{10} helix formation between β-strand 1 and H1 as in ARR has not been seen VRQ simulations.

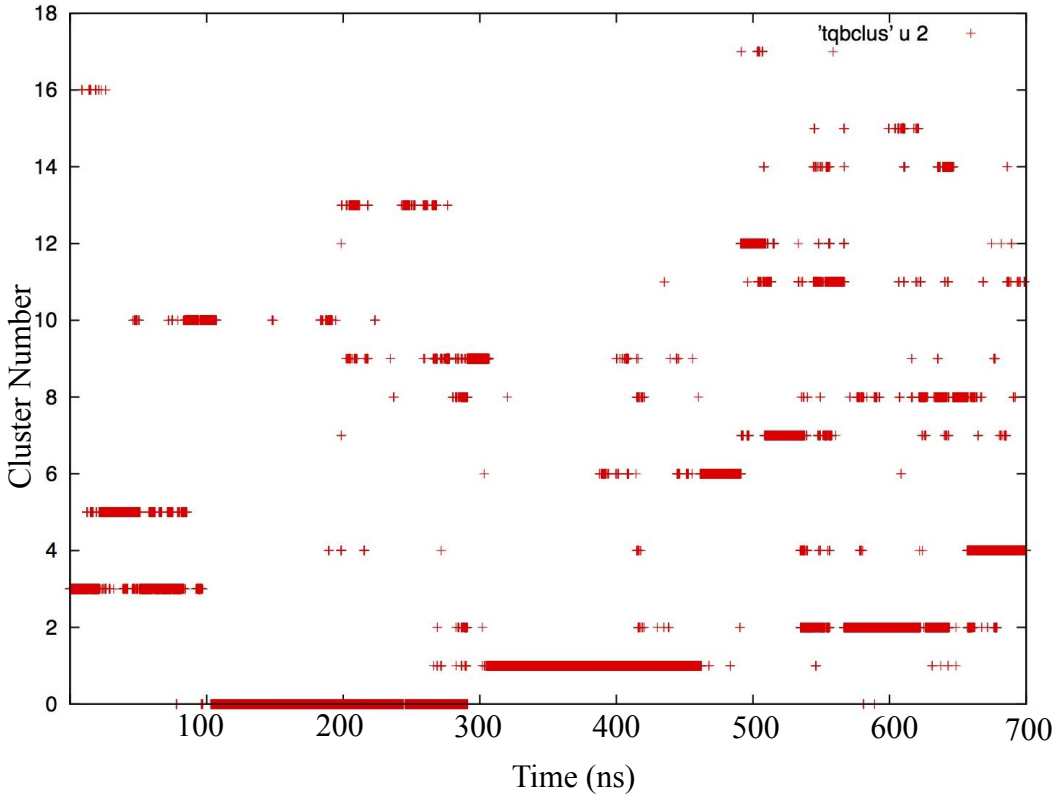

Figure 3.16 : Clusters and Cluster Members of VRQ with respect to time.

3.2 Detailed Analysis of the Simulations at 310K

3.2.1 The effect of Q/R variation at position 171

There is no major effect observed in simulations due to the identity of Q171. The region around this residue is similar in all three simulations. In the literarture it was found that substitution of neighbouring Y172 (Y169 in mouse) by glycine converted the helical turn in this region into a β-turn. This was proposed to result in the disease [31]. In our simulations, when there is an arginine at this position in ARR it makes a salt bridge with the neighboring D170. When there is a glutamine at this position in ARQ, either it makes a hydrogen bond with D170 or its side chain is oriented into the solution. The same is true for VRQ. In any case the structure of this region remains stable (Figure 3.17).

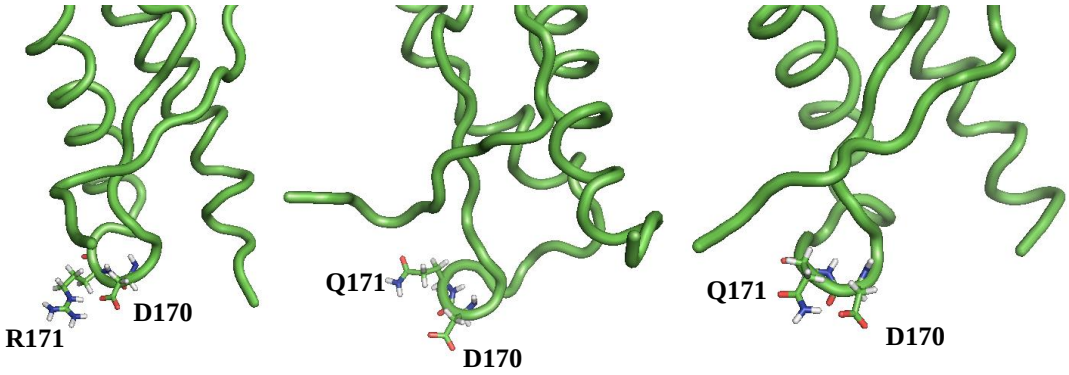

Figure 3.17 : Respectively ARR, ARQ, VRQ simulations and the positions of the residues D170 and R/Q171.

Since there is no effect observed in monomer simulations, this residue may be effective in another stage of PrP^{Sc} formation such as in the oligomer formation by playing a role in the interface. Similarly, the differences between ARR and ARQ simulations are not expected to arise from the Q/R variations at position 171. If the simulations were prolonged the same behaviour would be expected in both simulations.

3.2.2 Structure of H1 and H1-B1 loop

The C-terminus of H1 is attached to the N-terminus of H3 via R159-D205 salt bridge in all simulations. Also in almost in all of the ARR and ARQ simulations Y160 makes a hydrogen bond with D205. This interaction is seen in the early stage of the VRQ simulation. This interaction connects the C-terminus of H1 to the N-terminus of H3.

In the crystallographic structure, the last turn of H1 is distorted. The strain caused by the distortion is compensated by several interactions between H1 and H3:

- Salt bridge between E149 and K207
- Hydrogen bond between Y152 and D205
- Hydrophobic contacts between I208, V212 on H3 and F144, Y153, I142 on H1 or H1-B1 loop.

Due to these interactions, the contact between H1, H1-B1 loop and H3 expands over a large surface, referred as closed conformation below (Figure 3.18).

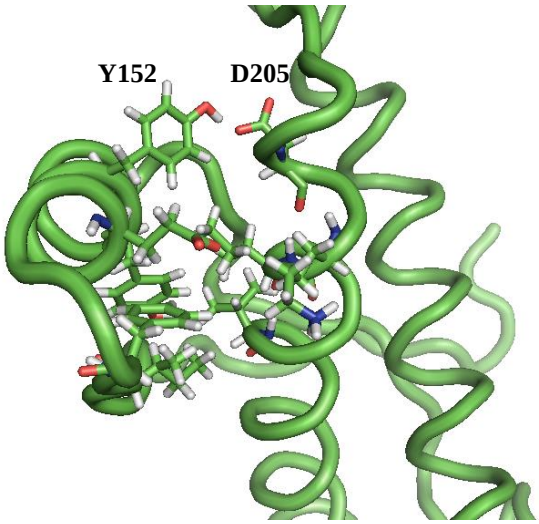

Figure 3.18 : Interactions between H1, H3 and H1-B1 H3 Loop in the crystallographic structure.

In the ARQ simulations, only the K207-E149 salt bridge disappears immediately at the beginning of the simulations. It is replaced by the E149-R211 salt bridge during the most of the simulations. Similarly, I142 is replaced by P140 while the remaining hydrophobic contacts have been conserved along the whole simulation (Figure 3.19). In addition, the Y152-D205 hydrogen bond is seen during almost all the simulation. As a result of these interactions, the distortion in H1 persists during the simulation and the close confirmation is observed.

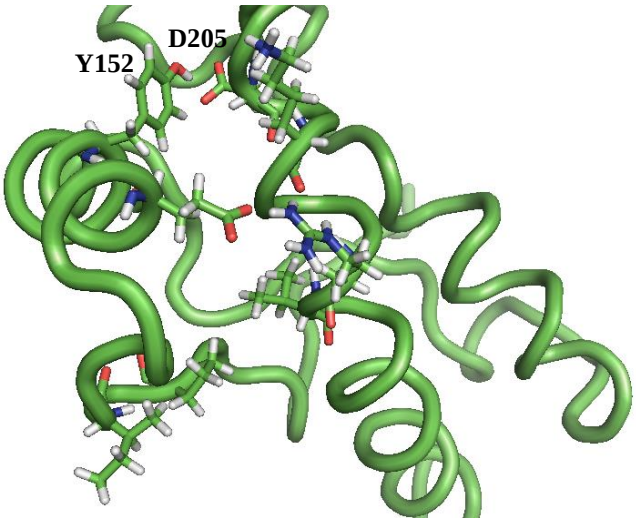

Figure 3.19 : Interactions in ARQ after K207-E149 and I142-V212 are replaced by E149-R211 and P140-V212.

The interactions between H1 and H3 inevitably causes a distortion in H1. This distortion is confined at the last turn because the R154-D150 and R151-D147 salt bridges maintain the stability of the other turns in all simulations. In rare moments where one of these interactions is absent, the corresponding turn is also distorted. In most part of the simulations R154 interacts also with D147, strengthening further H1. (Figure 3.20).

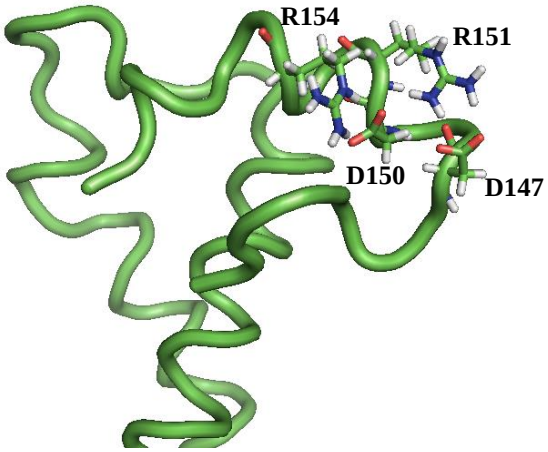

Figure 3.20 : R154-D150 and R151-D147 salt bridges maintain the stability of the N-terminal turns of H1.

Unlike ARQ, in ARR and VRQ, the distortion of H1 is removed by breaking some of the interaction between H1 and H3. This reduces the contact surface between H1 and H3, leading to an open conformation. In both cases the salt bridge between E149 and K207 disappears at the beginning of the simulations and is never reformed. Similarly hydrogen bond between Y152 and D205 also disappears at the beginning. While, the aromatic ring of Y152 interacts with H3 in some parts of the ARR simulation, this interaction has not been seen in VRQ simulation. The other interactions mentioned above also disappear and interactions which are explained below are seen.

At some parts of the ARR and VRQ simulations residues L141-N146 exhibit a 3_{10} helix structure. The formation of 3_{10} helix at VRQ and ARR is not seen at the early phase of the simulation because it is blocked by R154 which interacts with backbone oxygens of residues P140, L141 and/or I142 together with the side chain of D150 mentioned above. In addition hydrophobic contacts between F144 and H3 does not allow the backbone NH group of this residue adopt a suitable orientation for helix

formation. In ARQ simulations hydrophobic contacts between F144 and H3 persist, therefore helix formation has not been observed. However in ARR and VRQ, F144 loses its hydrophobic interactions by rotating its side chain towards the solvent. Consequently its backbone NH group reorients such that it can participate in the formation of the 3_{10} helix at this region.

At a later phase of the simulation R139 makes a salt bridge with the D150. Thus the 3_{10} helix formation is seen between residues L141-N146 (Figure 3.21). In the presence of the 3_{10} helix, mostly the salt bridge between R139 and D150 has been observed. We think that this interaction stabilizes 3_{10} helix.

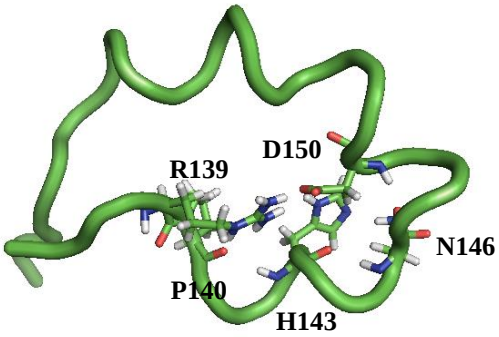

Figure 3.21 : Salt bridge between R139-D150 and formation of 3_{10} helix.

This structure is an open structure when it is compared with other structures during simulations. Both ARR and VRQ simulations show similar structures when 3_{10} helix is formed. Although most of interactions disappear, some interactions are still seen between H1 and H3 or H1-B1 loop and H3. Hydrophobic contacts between Y152 Y153 and I208 are seen between H1 and H3. Some interactions which are P140, I142 and Q215 are seen between H1-B1 loop and H3 (Figure 3.22). Also β-sheet is stable and maintains its interaction with H2 and H3.

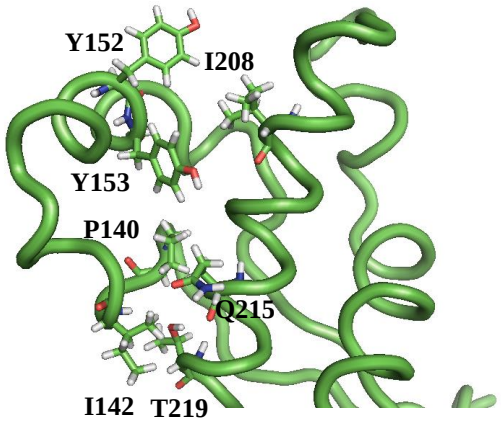

Figure 3.22 : Interactions between H1and H3 or H1-B1 loop and H3 when the 3_{10} helix is formed.

The 3_{10} helix is seen in frequently during ARR simulations and rarely in VRQ simulations.

The conformation which is seen only in the VRQ simulation is a very open structure where H1 is located away from H3. The last turn of the H1 is opened. The distance between H1 and H3 ossilates from open to very open. The hydrogen bond between Y160 and D205 is broken at very opened position. Only R159-D205, Y160-V212 and P140-V212 interactions are seen between H1and H3 or H1-B1 loop and H3 (Figure 3.23).

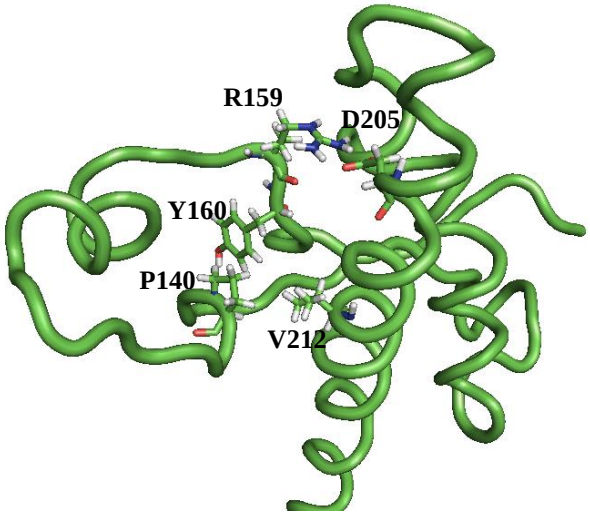

Figure 3.23 : Interactions in the very open conformation.

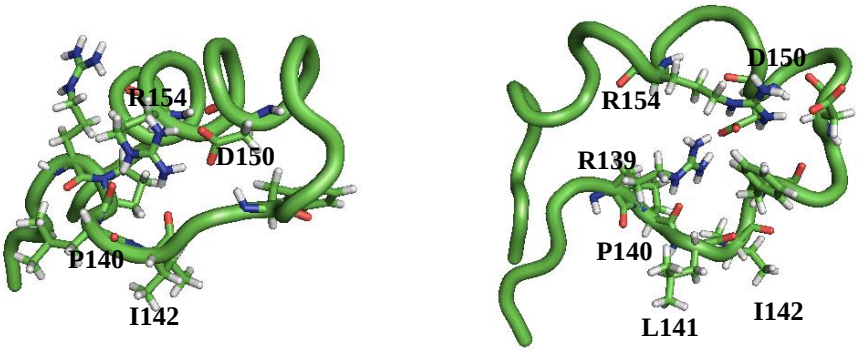

(A) (B)

Figure 3.24 : Interaction preventing (A) or favoring (B) the formation of 3_{10} helix.

A: R154 with backbone of P140, L141 and/or I142 together with the side chain of D150.

B: Interaction of R139 with the side chain of D150.

In summary;

There are 3 different conformation observed in the simulations.

1. Closed conformation: This conformation is observed along the whole simulation of ARQ and at early phases of ARR and VRQ simulations. 'Many' interactions are seen between H1 and H3. Also it is characterized with distortion of the last turn of H1.
2. Open conformation: The distortion of the last turn of H1 is not seen , some of the interactions between H1 and H3 are broken and mostly a 3_{10} helix conformation is seen in this conformation.
3. Very open conformation: This is only seen in VRQ simulation. H1 is located away from H3 and interactions between H1 and H3 are minimum in this conformation.

3.2.3 Structure of the β-sheet in the neighbourhood of A/V136

Alanine and valine are located in the ARR/ARQ and VRQ variants respectively. Locations of these residues show variations. Because alanine is a small residue, its side chain can fit into the space between M216 and Q220. In this conformation, in order to avoid steric interactions between side chain of A136 and backbone oxygen of S135, its backbone NH group is forced to be oriented towards N162 and

contributes to form longer β-sheet via hydrogen bonding (Figure 3.25). Alanine also displays another position in which it is partially exposed to the solution. In this way it is not able to contribute to the hydrogen bonding with N162. In this position it is seen mostly between Q220 and E224 (Figure 3.26). This conformation is stabilized by hydrogen bond between backbone of A136 and the side chain of Q220.

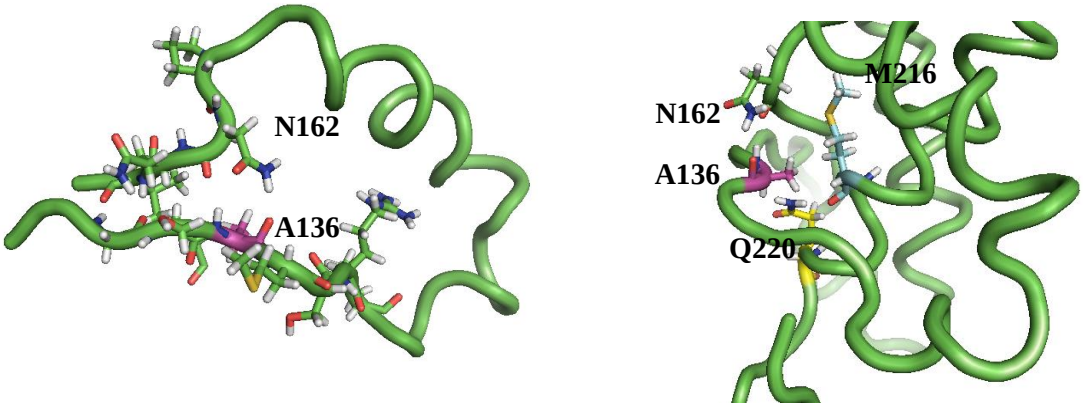

Figure 3.25 : Hydrogen bond between A136-N162. Alanin can fit into the space between M216 and Q220.

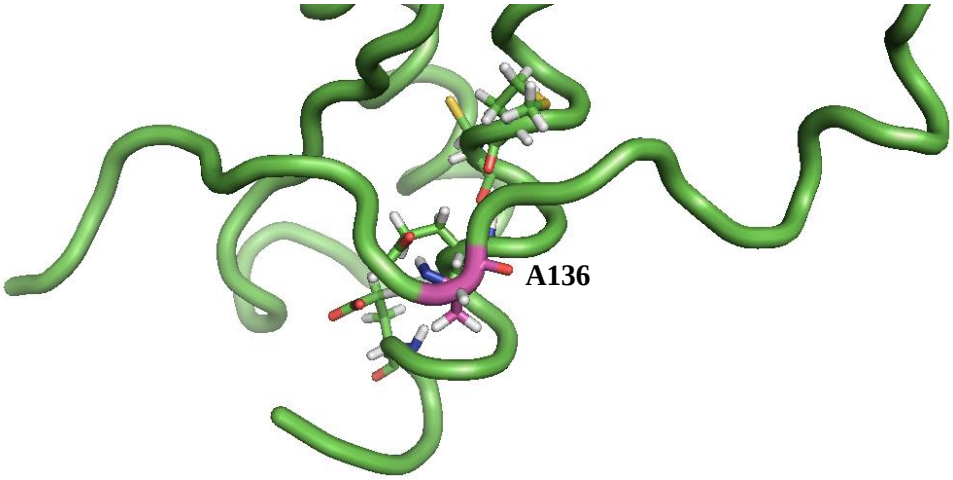

Figure 3.26 : Alanine in a partially solvent exposed conformation.

Alanine rarely shows fully solvent exposed conformation. Side chain turns into solvent. Therefore hydrogen bond is seen between N162 and NH group of M137 instead of A136. β-sheet is seen between between residues 137-162 (Figure 3.27).

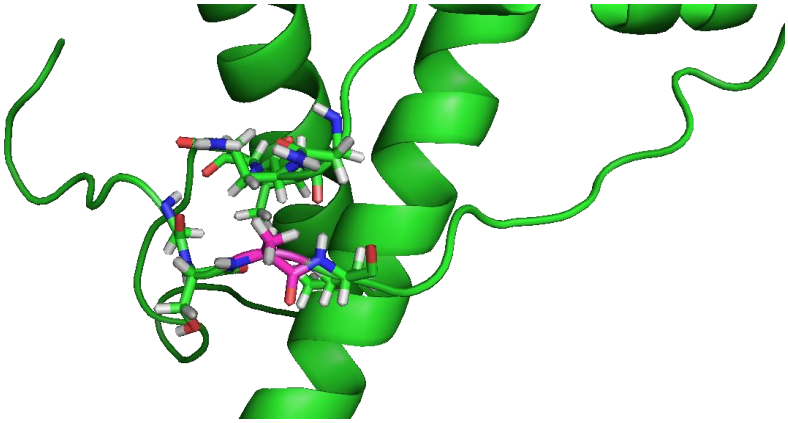

Figure 3.27 : Hydrogen bond is seen between N162 and NH group of M137 in fully solvent exposed conformation of alanine.

Unlike alanine, valine is not able to turn towards M216 and Q220 due to its large and branched structure. Therefore valine is observed mostly into the solution This conformation of alanine results with interactions of H1-B1 loop and H3. Also this alanine conformation contributes to form longer β-sheet. Probably these effects, stabilize the structure and prevent the moving away of H1 from H3 more. Turning the side chain of valine to solution has an advantage by decreasing the steric effects but it has a negative effect for hydrophobic group to be forced in the solution. This location of the valine causes to form a bulge and hydrogen bonding between M137 and N162 thus it contributes to form a longer β-sheet. Neighbouring M137 is seen that it can fit the space where valine is not able to fit inside, due to the branched structure of valine although methionine is bigger than valine (Figure 3.28). At this position H1 shows open conformation.

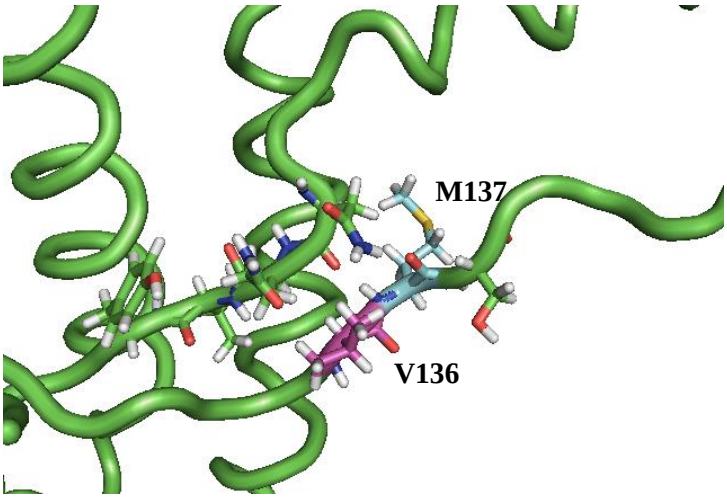

Figure 3.28 : V136 located in the solution.

The other fully solvent exposed conformation of valine is only seen in 'very open conformation' of H1. β turn is observed between NH group of S138 and CO group of S135 instead of hydrogen bonding between M137 and N162 (Figure 3.29).

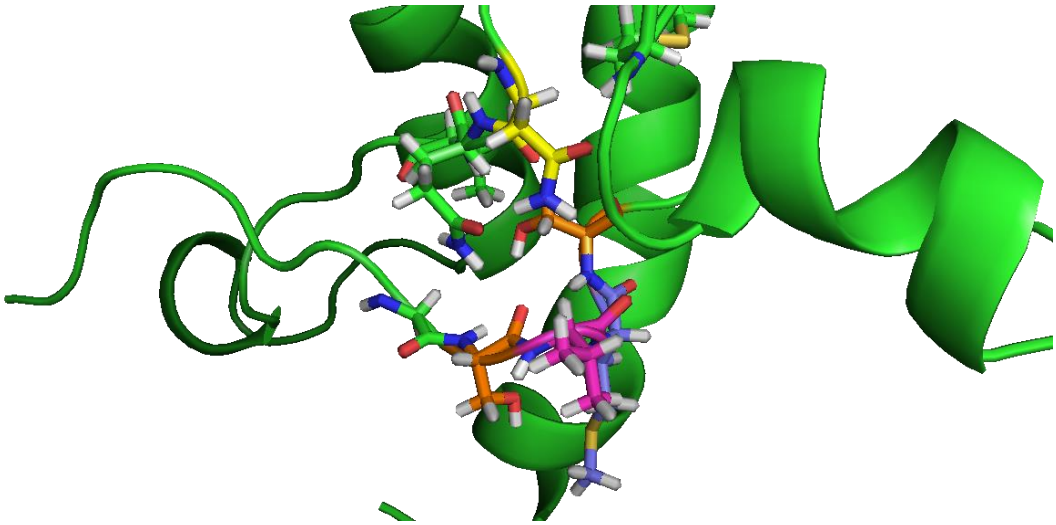

Figure 3.29 : β turn formation in very open conformation.

Valine can change its position to the partially exposed conformation which is also seen in alanine conformation. CO group of valine is toward solution in order to prevent steric interaction. NH group of M137 is toward to H3. There is a hydrogen bond between M137-Q220. In the presence of alanine, this hydrogen bond is formed by alanine instead of methione (A136-Q220) for its side chain is not as large as valine.

In the very open conformation with partially solvent exposed valine, valine is able to form hydrogen bond between Q220 at the expense of turning CH3 group into solvent (Figure 3.30).

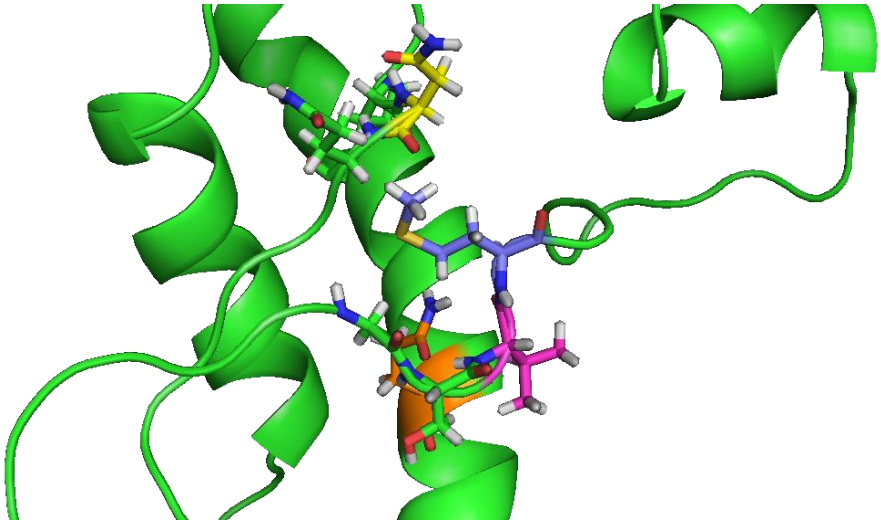

Figure 3.30 : Hydrogen bond is between Q220 and V136 in very open conformation of valine.

Also hydrogen bond can be seen between M137 and Q220 if V136 is not able to forms hydrogen bonding with Q220 in this conformation (Figure 3.31).

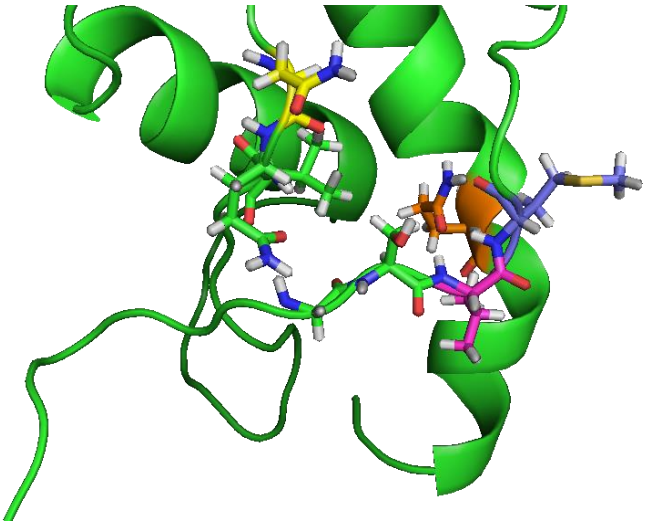

Figure 3.31 : Hydrogen bond is between M137 and Q220.

Sometimes hydrogen bonding is seen between S138 and N162 or some hydrophobic interactons are observed between Y160 and P140 in this conformation (Figure 3.32, Figure 3.33).

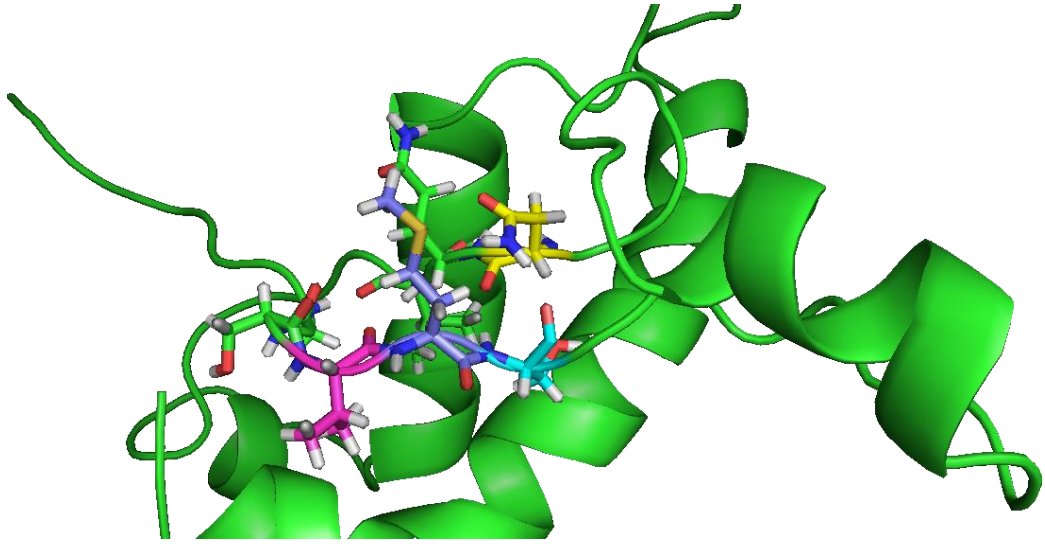

Figure 3.32 : Hydrogen bond is between S138 and N162.

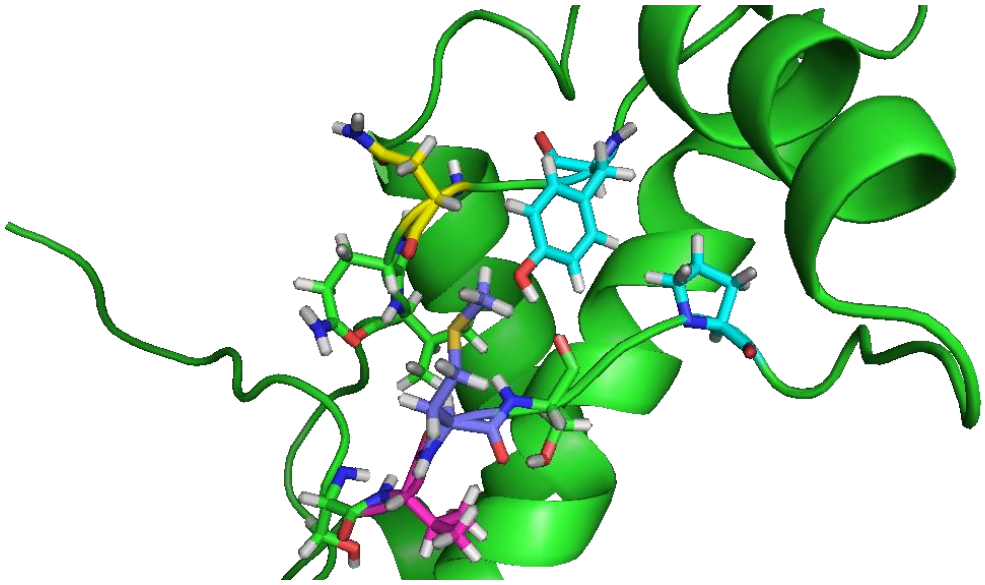

Figure 3.33 : Hydrophobic interactions are between Y160 and P140.

Valine is rarely observed in buried conformation. This conformation only seen in 'very open' conformation of H1. At the expense of increasing distance between H1 and H3, valine can fit this space (Figure 3.34).

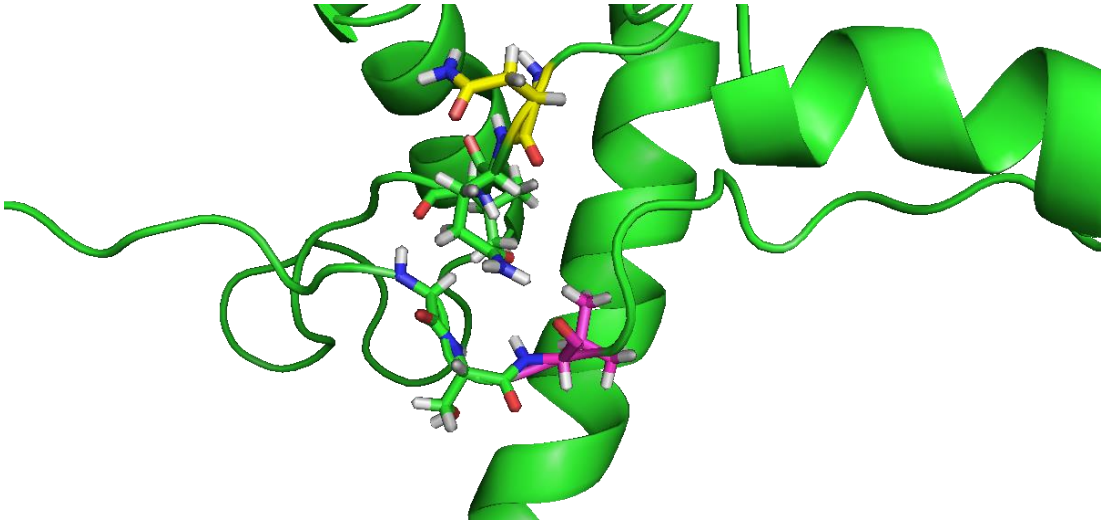

Figure 3.34 : Valine in the burried conformation in very open conformation.

Unwinding the last turn of H1 increases the flexlibility of H1 and H1-B1 loop. This results in the very open conformation which is not seen in alanine simulation. Before unwinding of the last turn of H1, fully solvent exposed and partially exposed conformations of valine are stable enough to be observed for 200ns. However addinitonal conformations are observed with increasing flexibility of H1 and H1-B1 loop after unwinding last turn of H1.

3.2.4 The banana peeling model and current simulations

Disease is related with H2 and H3 according to the 'Banana peeling model':

According to this model, H2 and H3 are converted to β-sheets and are the aggregation seed that is directly involved in fibrillogenesis of PrP. Prior condition for this model is that H1 (banana skin) should be removed in order to expose H2 and H3 to promote conversion from a helical to β-rich structure[49]. In our study H1 mobility and deformation have been observed. Therefore we believe that this supports to the 'Banana peeling model.'

Therefore we have simulated only H2-H3. It is seen that H2-H3 are unstable without H1 (Figure 3.35).

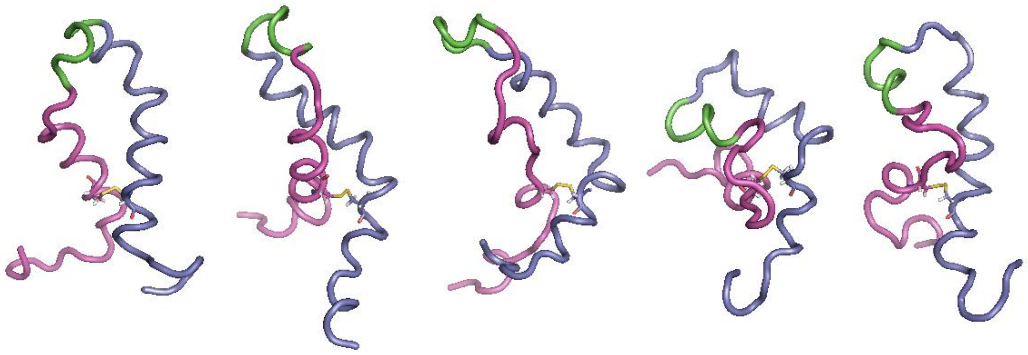

Figure 3.35 : H2, H3 and H2-H3 loop during simulation.

β-sheets have not been observed in this simulation because of absence of PrP^{Sc} template in our simulation.

In ARR and ARQ simulations, H1 is close to H2 and H3 thus it maintains the integrity of H2 and H3. In VRQ simulation, H1 moves away from H3 notably. Although we have not seen the β-sheet formation on H2 and H3 in this simulation, we have seen that unstable H2 and H3 are appropriate for this formation. Therefore our results corroborate with 'Banana peeling' model and explain the difference of susceptibility of three different variants.

3.3 Additional Simulations at 310K

3.3.1 Restrained simulations forcing β-sheet formation

Although rarely, flexibility of the residues 186-204 leads to the formation of a hairpin in this region or these residues approach to the C-terminus of H1. Some backbone oxygens start to have an interaction with backbone NH groups in this region. Therefore we have examined the possibility of the formation of β-sheet due to these interactions. Restraints have been applied on these interactions and have been simulated. Snapshots of these simulations are given below (Figure 3.36, Figure 3.37) Unfortunately β-sheets have not been extended beyond the restrained region.

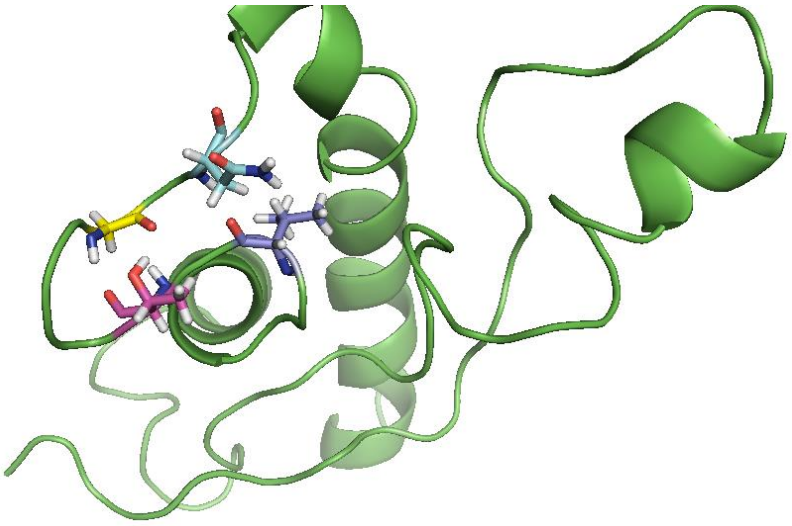

Figure 3.36 : Restrained regions in VRQ : 1) G198 NH – T194 CO (yellow-pink) 2) G198 CO – T194 NH 3) N200 NH – V192 CO (blue-purple)

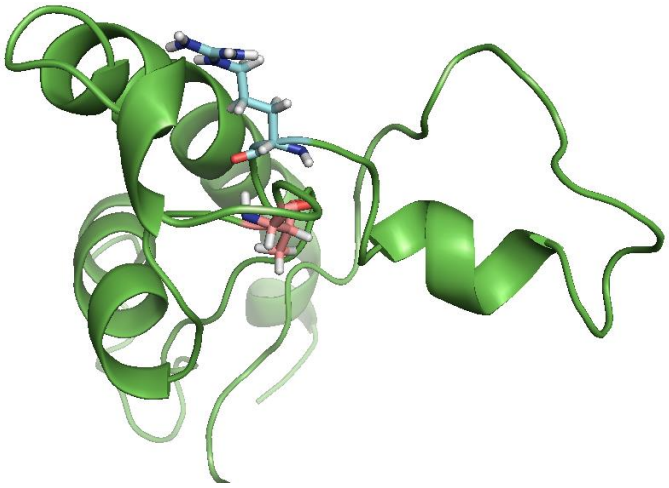

Figure 3.37 : Restrain regions in VRQ: 1) R159 CO – T194 NH (blue-salmon) 2) R159 NH – T194 CO

3.3.2 A136V mutation in ARR and V136A mutation in VRQ

We have performed new simulations starting with snapshots in ARR and VRQ simulations and mutating A136 to valine or vice versa in order to observe the effects of A136V or V136A. We have observed that V136 shows same properties with A136 in the early stage of A136V simulation; V136 is located as A136 where its backbone NH group is forced to be oriented towards N162 and contributes to form longer β-sheet via hydrogen bonding and it is seen mostly between Q220 and E224. Partially exposed conformation of alanine has also been observed in A136V simulation. Conformations which is only seen in valine simulations are observed after 160ns. A136V is seen mostly into the solution as in VRQ simulation. The other specific

conformations for alanine is seen rarely in the rest of the simulation. We have not observed the very open conformation and the unwinding of last turn of H1 in A136V simulation. We believe that when the simulation are performed long enough, very open conformation and the unwinding of last turn of H1 can be observed.

We also have observed the same results for our V136A simulation. Valine effects are seen in the early stage of simulation due to short simulation. (100ns) We believe that longer simulations are needed in order to observe totally alanine effects in this simulation.

3.4 Simulations at 330K

All simulations of ARR, ARQ and VRQ pass the activation barrier for the conformational motion of H1 and have high mobility at 330K. H1 moves towards the C-terminus of H3 in all three simulations. The original β-sheet is broken down only in the VRQ simulation. Structures of ARR and ARQ at 330K are similar to the structure of VRQ at 310 K. H1 rotates away from H3 but there is no deformation in the original β-sheet unlike in VRQ simulations in 330K.

We do not know whether there will be any deformations of the original β-sheet following the movement of H1 away from H3 in ARR and ARQ simulations as observed in VRQ simulation. Longer simulations are needed to shed light on this point.

H1 fluctuations in ARR and ARQ are smaller, indicating that rotation of H1 away from H3 or its movement towards the C-terminus of H3 have a high barrier. On the other hand the barrier can be overcome in VRQ simulations in 310 K. Our data is not enough to say conclusively that these conformational changes are on pathway or off pathway to PrP^{Sc} formation. Nevertheless, the fact that the conformational changes are seen mostly in VRQ which is the variant most susceptible to scrapie instead of ARR and ARQ (more resistant variants) makes us think that these changes are on pathway.

4. CONCLUSION AND RECOMMENDATIONS

Transmissible spongiform encephalopathies (TSEs) are fatal neurodegenerative disorders. These are the main cause of several diseases such as Creutzfeldt–Jakob Disease, fatal familial insomnia, Gerstmann- Straussler-Scheinker syndrome in humans and scrapie, bovine spongiform encephalopathy, transmissible mink encephalopathy in several species.

The reason of these diseases is an abnormal isoform of the protein PrP^{C} which is called PrP^{Sc}. Transition of PrP^{C} to PrP^{Sc} ends up with TSEs. PrP^{Sc} can act as a template for the accelerated conversion of another PrP^{C} to PrP^{Sc}. This misfolding leads to form aggregates, fibrillar filaments, fatal plaques. Misfolding pathways of TSE diseases should be elucidated for both human-community health care and livestock farming and economy. Scrapie is the most common TSE diseases of livestock in the world. Therefore we aimed to understand prion misfolding pathways by using MD simulations.

Simulations have been carried out on three different variants ARR, ARQ, VRQ in 310 K and 330 K. Fluctuations are mostly seen in RMSD and B-factor graphs of VRQ (the most susceptible variant) than ARR and ARQ (more resistant variants). It has been seen that H1 rotates away from H3 or move towards to C terminus of H3 in VRQ. Also residues 186-204 have high mobility.

The other variants have less fluctuations or mobility that rotate H1 away from H3. Compared to ARQ, residues 186-204 have not fluctuated significantly in ARR. If fluctuations in ARQ in this region are compared with VRQ , they are less.

There are 3 different conformation observed in the simulations.

1. Closed conformation: ‘Many’ interactions are seen between H1 and H3. Also it is characterized with distortion of the last turn of H1.

2. Open conformation: The distortion of the last turn of H1 is not seen , some of the interactions between H1 and H3 are broken and mostly a 3_{10} helix conformation is seen in this conformation.
3. Very open conformation: This is only seen in VRQ simulation. H1 is located away from H3 and interactions between H1 and H3 are minimum in this conformation.

A136 is able to turn toward to M216 and Q220 therefore it contributes to form longer β-sheet and more interactions H1-B1 loop and H3. Therefore stabilizes the structure. Valine is not able to turn toward M216 and Q220 therefore it acquires either a fully solvent exposed conformation or partially exposed conformation. In the fully exposed conformation location of the V136 cause to form a bulge then hydrogen bonding between M137 and N162 thus it contribute to form longer β-sheet. Both conformations are also observed before and after the unwinding the last turn H1.

H1 mobility is seen in all simulations (ARR, ARQ, VRQ) at 330K. Therefore this activation barrier can be passed by high temperature by ARR and ARQ which displayed lower H1 mobilities at 310K. In addition the original β-sheet is deformed at 330 K in VRQ simulations.

In the literature; movement of H1 away from H2 and H3 is assumed to be the first step of the β-sheet formation of H2 and H3 which is called as "banana peeling model" [49].

H1 mobility and rotations in our simulations are considered to be the initial step of the 'banana peeling model'. Therefore simulations can be extended to confirm this idea. Restraints can be used at different regions in order to enhance the β-sheets formation. Replica Exchange Molecular Dynamics or Accelerated Molecular Dynamics methods which accelerate the conformational changes can be used in order to see more conformations.

REFERENCES

[1] **Cassard, H., Torres, J.M. and Lacroux, C.** (2014). Evidence for zoonotic potentaial of ovine scrapie prions, *Nature Communications*, 5.

[2] **Prusiner, S. B.** (1998). Prions. *Proc. Natl. Acad. Sci. U.S.A.* 95, 13363–13383

[3] **Caughey B.W., Dong, A., Bhat, K.S., Ernst, D., Hayes, S.F., Caughey, W.S., (**1991). Secondary structure analysis of the scrapie-associated protein PrP 27–30 in water by infrared spectroscopy, *Biochemistry*, 30, 7672–7680.

[4] **Safar, J., Roller, P.P., Gajdusek, D.C. and Gibbs Jr, C.J.,** (1993). Conformational transitions, dissociation, and unfolding of scrapie amyloid (prion) protein, *J. Biol. Chem*, 268, 20276–20284.

[5] **Dickinson, A.G. and Meikle, V.M.** (1969). A comparison of some biological characteristics of the mouse-passaged scrapie agents, 22A and ME7, *Genet. Res.*, 13, 213–225.

[6] **Fraser, H., Bruce, M.E. and McConnell, I.** (1991). Murine scrapie strains, BSE models and genetics, in: R. Bradley, M. Savey, B. Marchant (Eds.), Sub-acute Spongiform Encephalopathies, Kluwer, Dordrecht, 131–136.

[7] **Groschup, M.H. and Kretzschmar H.A. eds.** (2001). Prion Diseases Diagnosis and Pathogeneis, *Archives of Virology*, Suppl 16 (New York: Springer).

[8] **Brown, P. and Gajdusek, D.C.** (1991). Survival of scrapie virus after 3 years' interment. *Lancet*, 337 (8736), 269-270.

[9] **Johnson, C.J., Phillips, K.E., Schramm, P.T., McKenzie, D., Aiken, J.M. and Pedersen, J.A.** (2006). Prions adhere to soil minerals and remain infectious. *PLoS Pathogen*, 2 (4), e32, Epub.

[10] **Healy, A.M., Hannon, D., Morgan, K.L., Weavers, E., Collins, J.D. and Doherty, M.L.** (2004). A paired case-control study of risk factors for scrapie in Irish sheep flocks. *Prev. vet. Med*, 64 (2-4), 73-83.

[11] **Detwiler, L.A.** (1992). Scrapie. In Transmissible spongiform encephalopathies of animals (R. Bradley & D. Matthews, eds). *Rev. sci. tech. Off. int. Epiz*, 11 (2), 491-537.

[12] **Philippe, S., Ducrot, C., Roy, P., Remontet, L., Jarrige, N. and Calavas, D.** (2005). Sheep feed and scrapie, *France. Emerg. infect*. Dis., 11 (8), 1274-1279.

[13] **Ironside, JW; Sutherland, K; Bell, JE; McCardle, L; Barrie, C; Estebeiro, K; Zeidler, M; Will, RG** (1996). "A new variant of Creutzfeldt–

Jakob disease: neuropathological and clinical features.". *Cold Spring Harbor symposia on quantitative biology 61*: 523–30.

[14] **Lugaresi, E; Medori, R; Montagna, P; Baruzzi, A; Cortelli, P; Lugaresi, A; Tinuper, P; Zucconi, M; Gambetti, P** (Oct 16, 1986). "Fatal familial insomnia and dysautonomia with selective degeneration of thalamic nuclei". *The New England Journal of Medicine 315* (16): 997–1003

[15] **Niimi Y, Iwasaki Y, Umemura T** (December 2008). "MM2-cortical-type sporadic Creutzfeldt–Jakob disease with early stage cerebral cortical pathology presenting with a rapidly progressive clinical course". *Neuropathology 28* (6): 645–51.

[16] **Sigurdsson, B.** (1954). Rida, a chronic encephalitis of sheep, with general remarks on infections which develop slowly and some of their special characteristics. *Br. vet. J.*, 110, 341-354.

[17] **Alper, T., Cramp, W.A., Haig, D.A. and Clarke, M.C.** (1967). Does the agent of scrapie replicate without nucleic acid? *Nature*, 214 (90), 764-766.

[18] **Prusiner, S.B.** (1982). Novel proteinaceous infectious particles cause scrapie. *Science*, 216 (4542), 136-144.

[19] **Donne, D. G., Viles, J. H., Groth, D., Mehlhorn, I., James, T. L., Cohen, F. E., Prusiner, S. B., Wright, P. E. and Dyson, H. J.** (1997). Structure of the recombinant full-length hamster prion protein PrP(29–231): the N terminus is highly flexible. *Proc. Natl. Acad. Sci. U.S.A.* 94:13452–13457.

[20] **Pastore, A., and Zagari, A.** (2007) *Prion 1*, 185–197

[21] **Prusiner, S.B.** (1991). Molecular biology of prion diseases, *Science,* 252, 1515–1522.

[22] **Pan, K.M., Baldwin, M., Nguyen, J.** (1993). Conversion of alpha helices into β-sheets features in the formation of scrapie prion proteins, *Proc. Natl. Acad. Sci. USA*, 90, 10962–10966.

[23] **Riek, R., Hornemann, S., Wider, G., Billeter, M., Glockshuber, R. and Wuthrich, K.** (1996). NMR structure of the mouse prion protein domain PrP(121–231). *Nature (Lond.),* 382, 180–182.

[24] **Riek, R., Hornemann, S., Wider, G., Billeter, M., Glockshuber, R. and Wuthrich, K. (**1997). NMR characterization of the full-length recombinant murine prion protein, mPrP(23–231). *FEBS Lett*, 413, 282–288.

[25] **Caughey, B. W., Dong, A., Bhat, K. S., Ernst, D., Hayes, S. F. and Caughey, W. S.** (1991). Secondary structure-analysis of the scrapie-associated protein PrP 27–30 in water by infrared spectroscopy. *Biochemistry*, 30, 7672–7680.

[26] **Gasset, M., Baldwin, M. A., Fletterick, R. J. and Prusiner, S. B.** (1993). Perturbation of the secondary-structure of the scrapie prion protein under conditions that alter infectivity. *Proc. Natl. Acad. Sci. U.S.A.* 90, 1–5.

[27] **Silveira, J. R., Raymond, G. J., Hughson, A. G., Race, R. E., Sim, V. L., Hayes, S. F., and Caughey, B.** (2005) The most infectious prion protein particles. *Nature* 437, 257−261.

[28] **Wille, H., Michelitsch, M. D., Guenebaut, V., Supattapone, S., Serban, A., Cohen, F. E., Agard, D. A., and Prusiner, S. B.** (2002) *Proc. Natl. Acad. Sci. U.S.A.* 99, 3563–3568

[29] **Govaerts, C., Wille, H., Prusiner, S. B., and Cohen, F. E.** (2004) *Proc. Natl. Acad. Sci. U.S.A.* 101, 8342– 8347

[30] **Heller, J., Kolbert, A. C., Larsen, R., Ernst, M., Bekker, T., Baldwin, M., Prusiner, S. B., Pines, A., and Wemmer, D. E**. (1996) *Protein Sci.* 5, 1655–1661

[31] **Christen, B., Hornemann, S., Damberger, F. F., and Wu¨thrich, K.** (2009) *J. Mol. Biol.* 389, 833– 845

[32] **Kaneko, K., Zulianello, L., Scott, M., Cooper, C. M., Wallace, A. C., James, T. L., Cohen, F. E., and Prusiner, S. B.** (1997) *Proc. Natl. Acad. Sci. U.S.A.* 94, 10069 –10074

[33] **Ning L., Wang Q., Zheng Y., Liu H. and Yao X.** (2015) Effects of the A117V mutation on the folding and aggregation of palindromic sequences (PrP113–120) in prion: insights from replica exchange molecular dynamics simulations. *Mol. BioSyst*., 11, 647

[34] **Colacino S., Tiana G., Broglia R.A., Colombo G.** (2006) The determinants of Stability in the Human Prion Protein: Insights into Folding and Misfolding from the Analysis of the Change in the Stabilization Energy Distribution in Different Conditions. *PROTEINS: Structure, Function, and Bioinformatics*, 62:698–707.

[35] **Viçosa D., Campos S.R.R., Baptista A.M.,, Machuqueiro M.** (2011) Reversibility of Prion Misfolding: Insights from Constant-pH Molecular Dynamics Simulations. *Biochemistry*, 50, 1162−1173.

[36] **Zhang J., Wang F., Zhang Y.** (2014). Molecular dynamics studies on the NMR structures of rabbit prion protein wild type and mutants: surface electrostatic charge distributions. *Journal of Biomolecular Structure and Dynamics*, 33:6, 1326-1335.

[37] **Garrec J., Tavernelli I., Rothlisberger U.** (2013) Two Misfolding Routes for the Prion Protein around pH 4.5 PLoS Comput Biol 9(5): e1003057.

[38] **Dima R., Thirumalai D.** (2004) Probing the instabilities in the dynamics of helical fragments from mouse PrPC. *Pnas*, 101, 15335-15340.

[39] **Cosseddu G.M., Agrimu U., Pinto J., Schudel A.A.** (2007) Advances in Scrapie Research, *Rev. Sci. Tech.*, 26(3), 657-68.

[40] **Karplus, M. and McCammon, A. J**. (2002) Molecular Dynamics Simulations of Biomolecules, *Nature Structural Biology*, 9, 646-652.

[41] **Boyd, D. B., Lipkowitz, K. B.,** (1982) Molecular Mechanics - The Method and Its Underlying Philosophy, *J. Chem. Ed*., 59, 269-274.

[42] **Rappe, A. K., Casewit, C. J., Colwell, K. S., Goddard III, W. A., Skiff, W. M.,** (1992) UFF, A Full Periodic-Table Force-Field For Molecular

Mechanics and Molecular Dynamics Simulations, *J. Am. Chem. Soc*., 114, 10024-10035.

[43] **Pearlman, D.A.; Case, D.A.; Caldwell, J.W.; Ross, W.S.; Cheatham, T.E. III; DeBolt, S.; Ferguson, D.; Seibel, G.; Kollman, P.** (1995). AMBER, a package of computer programs for applying molecular mechanics, nor- mal mode analysis, molecular dynamics and free energy calculations to simulate the structural and energetic properties of molecules. *Comp. Phys. Commun*., 91, 1–41

[44] **Case, D.A.; Cheatham, T.; Darden, T.; Gohlke, H.; Luo, R.; Merz, K.M. Jr.; Onufriev, A.; Simmerling, C.; Wang, B.; Woods, R.** (2005) The Amber biomolecular simulation programs. *J. Computat. Chem*., 26, 1668–1688.

[45] **Onufriev, A.; Bashford, D.; Case, D.A.** (2000) Modification of the generalized Born model suitable for macro- molecules. *J. Phys. Chem. B*, 2000, 104, 3712–3720.

[46] **Onufriev, A.; Bashford, D.; Case, D.A**. Exploring protein native states and large-scale conformational changes with a modified generalized Born model. *Proteins*, 2004, 55, 383–394.

[47] **Cramer, C.,** (2002) Essentials of Computational Chemistry: Theories and Models, John Wiley & Sons: New York.

[48] **Huang D., Caflisch A.** (2015), Evolutionary Conserved Tyr169 Stabilizes the β2-α2 Loop of the prion protein, *J.Am.Chem.Soc*, 137, 2948-2957.

[49] **Adrover M., Pauwels K., Prigent Stephanie, de Chiara C., Xu Z., Chapuis C., Pastore A. Rezaei H.** (2010) Prion fibrillization is mediated by a native structural elemnt that comprises helices H2 and H3, *J.Biol. Chem*, 285, 21004-21012

CURRICULUM VITAE

Name Surname: Fulya Ecem Keskin

Place and Date of Birth: Ankara 06.04.1989

E-Mail: fulyaecem@gmail.com

EDUCATION:

B.Sc.: Veterinary Faculty, Selçuk University, 2007-2012 (Graduated as honour student)

PROFESSIONAL EXPERIENCE AND REWARDS:

Second Manager, Inditex, Aug 2014 - …

Regulatory Specialist, Bavet, Jul 2013 - Aug 2014